

# Microengineering Pressure Sensor Active Layers for Improved Performance

Sara Rachel Arussy Ruth, Vivian Rachel Feig, Helen Tran, and Zhenan Bao\*

Pressure sensors play an integral role in a wide range of applications, such as soft robotics and health monitoring. In order to meet this demand, many groups microengineer the active layer—the layer that deforms under pressure and dictates changes in the output signal—of capacitive, resistive/piezoresistive, piezoelectric, and triboelectric pressure sensors in order to improve sensor performance. Geometric microengineering of the active layer has been shown to improve performance parameters such as sensitivity, dynamic range, limit of detection, and response and relaxation times. There are a wide range of implemented designs, including microdomes, micropylramids, lines or microridges, papillae, microspheres, micropores, and microcylinders, each offering different advantages for a particular application. It is important to compare the techniques by which the microengineered active layers are designed and fabricated as they may provide additional insights on compatibility and sensing range limits. To evaluate each fabrication method, it is critical to take into account the active layer uniformity, ease of fabrication, shape and size versatility and tunability, and scalability of both the device and the fabrication process. By better understanding how microengineering techniques and design compares, pressure sensors can be targetedly designed and implemented.

## 1. Introduction

Pressure sensors are playing an increasingly important role in a wide range of applications, from diagnostic health monitoring to precision surgery.<sup>[1–4]</sup> Next-generation monitoring devices have been reported that use pressure sensors to detect biological signals associated with health status, including blood flow,<sup>[5–10]</sup> tendon repair,<sup>[11]</sup> activity levels,<sup>[12]</sup> intraocular glaucoma progression,<sup>[13]</sup> catheters,<sup>[14]</sup> electronic or artificial skin,<sup>[12,15–24]</sup> and point-of-care immunoassays.<sup>[25]</sup> For example, a recent paper from our group demonstrated that arterial-pulse blood flow pressure sensors can be used for the early detection of failed vessel anastomosis—a surgical technique used to connect blood vessels—after complex reconstructive surgeries.<sup>[10]</sup> New

sensors are integral to be able to detect failure early because current technologies often do not detect failure until the graft can no longer be saved.<sup>[10,26,27]</sup> As tactile sensors,<sup>[18,28–36]</sup> pressure sensors that mimic cutaneous touch perception<sup>[15,37–40]</sup> may enable minimal access surgery,<sup>[41]</sup> humanoid robots,<sup>[37]</sup> human–machine interactions,<sup>[42–45]</sup> and biomimetic prostheses.<sup>[46]</sup> For instance, when combined with haptic displays, high performance pressure sensors can provide haptic feedback to surgeons to significantly improve the efficacy of minimal access surgical approaches that reduce recovery time, postoperative pain, tissue trauma, and length of hospital stay for patients.<sup>[41]</sup>


To meet the growing demand for tailored pressure sensors within the biomedical field, next-generation sensors aim to improve on the following key performance parameters: sensitivity, dynamic range, response time, relaxation time, and detection limit. Sensitivity describes how the

output signal changes relative to the initial output signal over a particular pressure range.<sup>[4,33]</sup> Quantitatively, sensitivity is the change in output signal divided by the initial output signal, which is further divided by the pressure change. High sensitivity is associated with higher signal-to-noise ratio, allowing the sensor to distinguish subtle changes in pressure.<sup>[4]</sup> For a sensor to properly transduce pressure signals, it must operate within a range of pressures—defined as the dynamic range—in which the signal response is detectable.<sup>[47,48]</sup> While a sensor may possess multiple linear regimes within the dynamic range, each with a corresponding sensitivity value, for the sake of consistency, we will focus this review mainly on each sensor's pressure range of highest sensitivity.

Response and relaxation times are critical parameters in determining the speed at which the sensor can be probed, which can be important for applications like pulse waveform evaluation, where the sensor must be able to respond quickly enough to accurately detect each beat. We define response time as the time it takes for a sensor to reach its final signal amplitude for an applied pressure, and relaxation time as the time it takes for the sensor to return back to its original signal once the applied pressure is removed.<sup>[47]</sup> It is important to note that when sensor response is rapid, evaluation of these parameters is typically limited by the equipment used to read out the sensor values; accordingly, response and relaxation times reported in literature may reflect equipment constraints rather than intrinsic sensor

S. R. A. Ruth, Dr. H. Tran, Prof. Z. Bao  
Department of Chemical Engineering  
Stanford University  
Stanford, CA 94305, USA  
E-mail: zbao@stanford.edu

V. R. Feig  
Department of Material Science and Engineering  
Stanford University  
Stanford, CA 94305, USA

 The ORCID identification number(s) for the author(s) of this article can be found under <https://doi.org/10.1002/adfm.202003491>.

DOI: 10.1002/adfm.202003491

performance. Finally, the detection limit is the minimum pressure that can be sensed, and is used to evaluate if a sensor is capable of detecting pressures for a given application.

This review will focus on pressure sensors that rely on the mechanical deformation of a sensor component to detect applied pressure or force normal to the sensor. The most common of these sensors utilize capacitive, resistive, piezoelectric, and triboelectric means to transduce said deformation into a measurable signal.<sup>[7,8,14,15,17,28,30,31,34,36,38,43,49–64]</sup> In all cases, the geometry of the active layer can have significant effects on a sensor's key performance parameters. A common approach to improve sensor performance involves changing the material used or engineering microstructures into the active layer with geometric features  $\approx 1\text{--}1000\text{ }\mu\text{m}$  in size. Since the former has been thoroughly addressed in literature,<sup>[33,65]</sup> this work will focus on the latter. Microengineered active layers include micropatterned structures, porous layers, multilayered packed structures, or a combination of these designs. Additionally, a variety of fabrication techniques have been reported for each of these designs. The advantages and limitations of these microengineering designs and fabrication methods depend on the specific sensing mechanism and target application (Figure 1).

In this review, we will discuss how microengineering is used to improve the performance of capacitive, resistive, piezoelectric, and triboelectric pressure sensors. For each sensor type, we will describe the sensing mechanism, including key equations, discuss geometric microengineering designs as well as their implications on sensor response to applied normal force, compare performance of reported examples in literature, discuss fabrication methods of the geometric microengineering designs, and compare sensor fabrication methods and techniques. Finally, we anticipate future needs of the field to efficiently meet the growing demand for new pressure sensors in the biomedical space.

## 2. Capacitive Pressure Sensors

Parallel plate capacitive sensors feature a dielectric between two electrodes and exhibit a change in the capacitance with applied pressure based on the change in distance between the two electrodes. They are designed using a simple governing equation:

$$C = \frac{\epsilon_r \epsilon_0 A}{d} \quad (1)$$

where  $C$  is the capacitance,  $\epsilon_0$  is the permittivity of free space,  $\epsilon_r$  is the relative permittivity,  $A$  is the overlapping area between the two electrodes, and  $d$  is the distance between the two electrodes.<sup>[66]</sup> Parallel plate capacitive sensors are commonly utilized because of their simple design and straightforward fabrication techniques.<sup>[67]</sup>

Capacitive pressure sensors are advantageous from several perspectives. From a performance standpoint, they exhibit high sensitivity and fast response times.<sup>[67]</sup> They have been demonstrated to recapitulate skin-type sensing behavior in terms of strain sensitivity, pressure, and proximity sensing.<sup>[30,31,58–60]</sup> Moreover, capacitive pressure sensors have low power consumption and can be made temperature-independent.<sup>[33,67]</sup> However, capacitive pressure sensors are susceptible to external noise sources from electromagnetic waves and high hysteresis



**Sara Rachel Arussy Ruth** graduated with a B.S. in Chemical Engineering from University of Maryland, Baltimore County in 2016 and an M.S. in Chemical Engineering from Stanford University in 2019. She is currently a Ph.D. candidate in Chemical Engineering under the supervision of Prof. Zhenan Bao. Her current

research focuses on improving predictability of pressure sensor performance for more efficient implementation of new pressure sensors for specialized medical applications.



**Vivian Rachel Feig** is a Ph.D. candidate in the Materials Science and Engineering department at Stanford University, under the supervision of Prof. Zhenan Bao. She received a B.S. in Chemical Engineering from Columbia University in 2012 and then worked at ExxonMobil until 2015. Her current research focuses on developing soft, conductive materials for

stable long-term bioelectronic interfaces. Her research is funded through a National Defense Science and Engineering Graduate Research Fellowship.



**Zhenan Bao** is a Professor of Chemical Engineering at Stanford University. Prior to joining Stanford in 2004, she was a Distinguished Member of Technical Staff in Bell Labs, Lucent Technologies from 1995 to 2004. She pioneered a number of design concepts for organic electronic materials. Her work has enabled flexible electronic circuits and displays. In her recent

work, she has developed skin-inspired organic electronic materials, which resulted in unprecedented performance or functions in medical devices, energy storage and environmental applications.

from unstructured rubber dielectrics due to their viscoelastic nature.<sup>[15,28,68]</sup> The latter can be improved upon by adding air gaps to the dielectric layer.<sup>[68,69]</sup>

Selecting the appropriate materials can enable capacitive pressure sensors to achieve improved functionalities like high

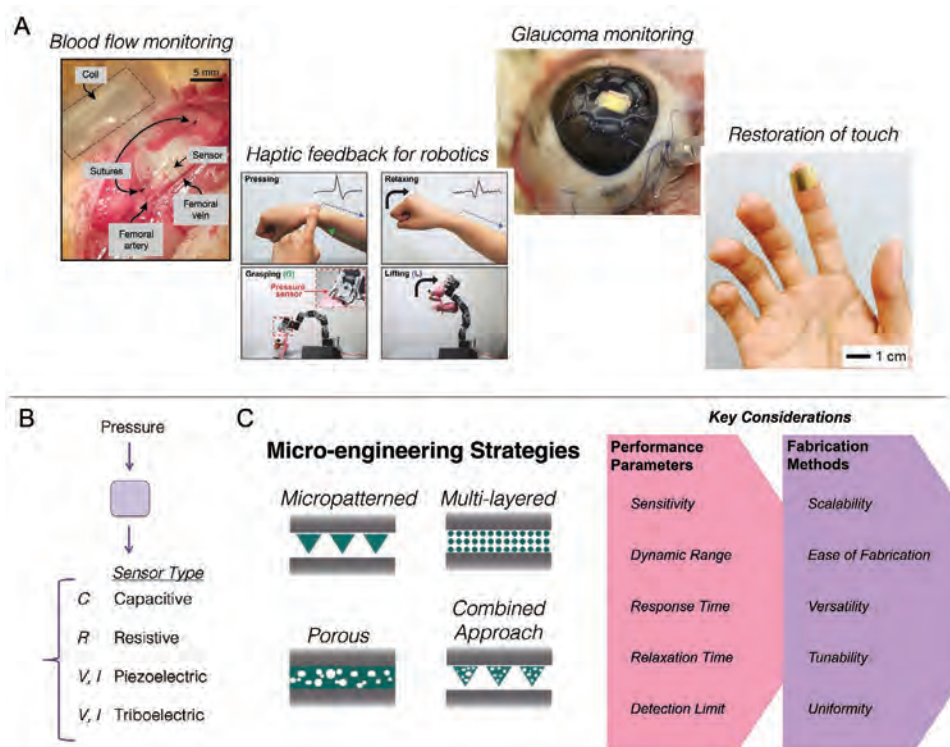


**Figure 1.** A) Pressure sensors are utilized in a wide range of applications in the biomedical field, including blood flow monitoring,<sup>[10]</sup> haptic feedback for robotics,<sup>[42]</sup> intraocular monitoring,<sup>[13]</sup> and restoration of touch.<sup>[18]</sup> Adapted with permission. Copyright 2019, Springer Nature; 2015, Wiley-VCH; 2008, IEEE; 2018, Wiley-VCH. B) Some of the most common pressure sensors include capacitive, resistive, piezoelectric, and triboelectric sensing mechanisms. C) Microengineering is used to improve performance of pressure sensors, but special considerations—scalability, active layer uniformity, performance predictability, shape and size versatility and tunability, and ease of fabrication—need to be taken into account for specific applications to choose the optimal technique.

stretchability, linearity, and even faster response times.<sup>[34,66,70]</sup> For example, stretchability can be improved using elastic materials. Further, sensor performance is easily tunable by changing the compressive modulus and dielectric constant of the dielectric material. In fact, using a simple model, our group has demonstrated that modulus has a much stronger effect on the sensitivity of the pyramid-structured capacitive pressure sensor than does the dielectric constant.<sup>[71]</sup> However, dielectric constant has a much stronger effect on the initial capacitance as compared to compressive modulus. With this in mind, there are limitations to the effect of modulus on sensitivity, including a potentially increased response time for softer materials from increased interfacial adhesion, which demands a more effective method of improvement.<sup>[17]</sup>

An increasingly popular approach to improve the performance of capacitive pressure sensors is to manipulate the geometry of the pressure-sensitive materials to enhance the compressibility of the dielectric layer.<sup>[15,67,71–74]</sup> When the dielectric layer is a bulk material, the applied pressure is converted to internal stress. By adding voids in the dielectric layer through microengineering, the layer can more readily deform with applied pressure, and consequently, can compress more easily (Figure 2A,B).<sup>[17,71]</sup> Since capacitance increases as the gap between the two electrodes decreases, microengineering improves sensitivity by allowing for greater changes in the interelectrode distance for a given applied pressure (Figure 2C–E). In addition,

the dielectric constant of the media changes with compression, which further enhances sensitivity. In general, increasing the compressibility of the dielectric layer will also increase the response time and detection limit. This is often accompanied by a decreased dynamic range, but this can be improved upon by making the dielectric layer thicker or by creating a dielectric layer that stiffens at higher pressures. Although the latter approach results in a lower sensitivity at higher pressures, it improves the dynamic range by increasing the range within which the sensor can detect pressure change. Finally, improved relaxation time can be achieved by reducing the viscoelasticity of the dielectric layer, which can also be achieved by microengineering (Figure 2F).

Several microengineering designs have been implemented for different applications, including micropatterned structures, porous layers, and combined approaches. In the following sections, we review these microengineering designs (Section 2.1) and discuss their advantages and disadvantages in terms of sensor performance (Section 2.2). We then describe reported fabrication methods that have been used to achieve these designs (Section 2.3), and discuss the implications of these approaches in terms of scalability, ease of fabrication, uniformity, versatility and tunability, and predictability (Section 2.4). In addition to intrinsic sensor performance, all of these considerations are important when deciding on a sensor design and fabrication route for a targeted application.



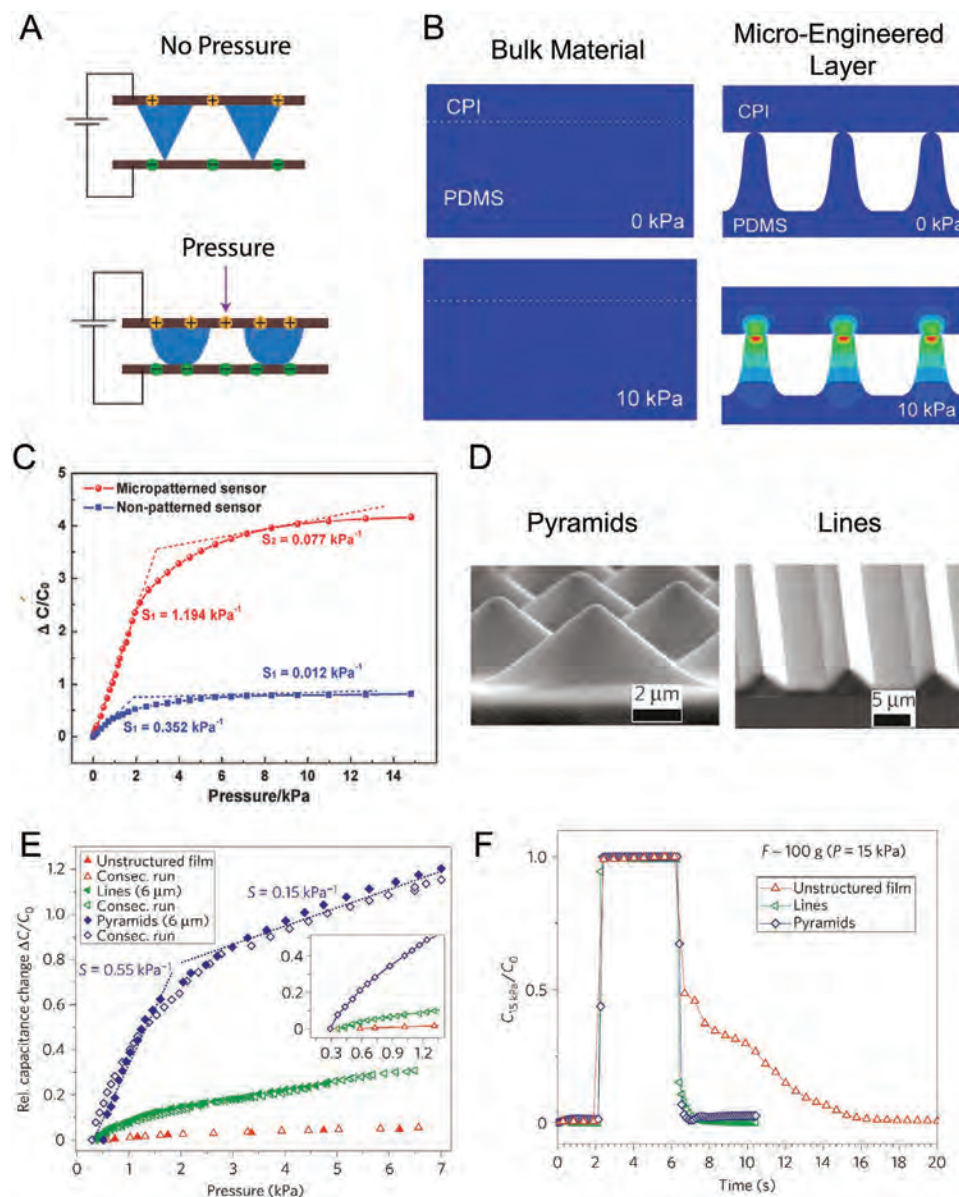


**Figure 2.** Advantages of microengineering the active layer of capacitive pressure sensors. A) When pressure is applied, the thickness of microengineered dielectric layers decreases and air is displaced. Adapted with permission.<sup>[148]</sup> Copyright 2016, Nature Publishing Group. B) Finite element simulation of bulk material and micro-towers with the same dielectric thickness demonstrate that microengineered layer compresses more than bulk material of the same thickness for a given applied pressure. Adapted with permission.<sup>[85]</sup> Copyright 2018, Wiley-VCH. C) The micropatterned sensor (Figure 4D) has a higher sensitivity in both high and low linear pressure regimes. Adapted with permission.<sup>[85]</sup> Copyright 2018, Wiley-VCH. D) SEM images of the pyramid and line micropatterns. Adapted with permission.<sup>[15]</sup> Copyright 2010, Macmillan Publishers Ltd. E) Pyramid microstructures (Figure 4A,G) demonstrate highly improved sensitivity as compared to unstructured films and line microstructures. Adapted with permission.<sup>[15]</sup> Copyright 2010, Macmillan Publishers Ltd. F) Pyramid and line microstructures (Figure 4A,G) demonstrate highly improved relaxation time as compared to unstructured films. Adapted with permission.<sup>[15]</sup> Copyright 2010, Macmillan Publishers Ltd.

## 2.1. Geometric Microengineering Designs for Capacitive Pressure Sensors

### 2.1.1. Micropatterned Structures

Micropatterning involves the controlled formation of micron-sized patterns in the sensor's dielectric layer, typically using a mold or standard lithographic processes.<sup>[15,75–77]</sup> Micropatterning decreases elastic resistance due to the aforementioned

air voids in the film, resulting in improved performance.<sup>[15]</sup> Further, the sensor sensitivity is increased because as the film is compressed, the displaced volume is air, which often has a lower dielectric constant than the elastomer.<sup>[15,71]</sup> Thus, in general, micropatterning the film increases the capacitance change for a given applied pressure by impacting both the distance change and the effective dielectric constant (Figure 2C).

Commonly used shapes for micropatterned structures include pillars, pyramids, and hemispheres, which can be

fashioned into arrays that vary in size and distribution throughout the sensor. The pyramid microstructure our group first proposed is widely used because of its nonuniform stress distribution, which concentrates at its pointed tip.<sup>[15,17,71,75,78]</sup> The tips of the pyramids will compress more for a given applied pressure, resulting in higher mechanical deformations, and consequently sensitivities, as compared to cubes or other microstructure shapes. For example, micropatterning PDMS dielectrics into micron-sized pyramids has been shown to improve sensitivity by over 30 times compared to non-patterned PDMS layers of equivalent dimensions (Figure 2D,E).<sup>[15]</sup> Micropatterning the dielectric layer also decreases the relaxation time of the compressed structure by several orders of magnitude, thereby minimizing problems associated with viscoelastic deformation, which can result in hysteresis and negatively impact response time (Figure 2D,F).<sup>[48]</sup> Micropatterned structures can also improve the detection limit by increasing the compressibility of the dielectric layer so that it deforms with lighter loads. In general, dynamic range decreases with micropatterning; however, choosing shapes such as the pyramid can mitigate this effect, since the shape change and stiffening of the pyramid upon compression can still yield a high pressure detection regime that is more sensitive than an unstructured sensor.<sup>[17]</sup>

The pyramid shape has been extensively studied using both finite element modeling (FEM) and computationally simpler methods.<sup>[17,71,77]</sup> FEM modeling confirms that pyramid shapes are more sensitive than both a flat film layer and a micropatterned layer comprising cuboid or cylinder shapes (Figure 3A,B).<sup>[77]</sup> Moreover, FEM has contributed to our understanding of how the sizes of the pyramid structures influence the performance of capacitive pressure sensors. For instance, Deng et al. demonstrated using COMSOL Multiphysics models based on FEM that making the base of the pyramid wider relative to its height decreases the sensitivity of the sensor.<sup>[77]</sup> Further, our group used FEM to identify the optimal side angle for the microstructure shape as 54.7° (Figure 3C).<sup>[17]</sup>

Beyond FEM, we also developed and experimentally validated a computationally simpler method to model the relationship between a wide range of dielectric layer geometric parameters and sensitivity.<sup>[71]</sup> We model the dielectric layer as a series of springs and capacitors in order to understand how capacitive pressure sensors will be affected mechanically and electrically in response to a given applied pressure.<sup>[71]</sup> Through this work, it is clear that sensitivity decreases as microstructures become more cuboid-like.<sup>[71]</sup> In fact, changing the pointedness of the pyramid microstructure while maintaining the side angle can change the sensitivity by several orders of magnitude, highlighting the importance of the pointed pyramid shape.<sup>[71]</sup>

Through our simple computational model, we demonstrated that both the distance between the pyramid microstructures along with the size of the pyramids are important control parameters in sensor performance. As interstructural spacing increases, the dielectric layer becomes more compressible since there is a higher percentage of air voids relative to elastomer. Subsequently, the sensitivity increases.<sup>[17,71]</sup> From this, it is clear that not only does the micropatterned pyramid structure improve the performance of capacitive pressure sensors, but it also can be easily tuned for various applications with simple design changes.<sup>[71]</sup>

In recent years, there has also been increased interest in micropatterning the electrode instead of the dielectric layer.<sup>[16,45,76,79–83]</sup> The rationale behind this design is analogous to micropatterning the dielectric layer. Compared to a flat electrode, under the same external pressure, the sensor made with a micropatterned electrode deforms significantly more due to the added compressibility, bringing the electrodes closer together (Figure 3D).<sup>[80]</sup> When the electrode is micropatterned, the applied pressure also increases the electrode area, which further increases the capacitance change and sensitivity.<sup>[45,80]</sup> Several structures have been used to micropattern the electrode for capacitive pressure sensors, including wrinkled line patterns, microtowers, microdomes, and cylinder shapes.<sup>[45,76,80,84,85]</sup> The wrinkled line pattern is similar to the inherent wrinkles in human skin and are often achieved by prestraining PDMS.<sup>[76]</sup> High aspect ratio microtowers and cylindrical columns incorporated into the electrode similarly can enhance the distance available for compression, resulting in higher sensitivities (Figure 3E).<sup>[85]</sup>

Finally, microstructure uniformity can also impact sensor performance, according to Chhetry et al.<sup>[86]</sup> Nonuniformity of the structures throughout a single micropatterned layer results in nonuniform response, since some of the microstructures will experience higher applied stress due to their different heights and shapes (Figure 3F). As such, the stress required to deform this layer is lower than would be required to deform a uniformly shaped micropattern of similar dimensions (Figure 3G). This means that having nonuniformity in a single-layer micropattern may be advantageous to produce sensors with greater deformation for a given applied pressure, and therefore higher sensitivities.<sup>[86]</sup> However, it is important to note analysis assumes the electrode remains flat with the applied pressure, something that may not be the case with flexible substrates.

### 2.1.2. Porous Layers

Beyond micropatterned structures, porous layers have become an increasingly popular way to microengineer the dielectric layer.<sup>[20,87–89]</sup> Micropores are air voids 1–1000 µm in diameter introduced to the dielectric layer, generally using either a template or by dissolving a material such as sugar once the elastomer layer has cured. As with micropatterned structures, the major advantage of porous layers is the increased compressibility of the dielectric layer due to the introduction of air voids, which have a lower dielectric constant and no resistance to deformation. This results in a higher capacitance change and, consequently, sensitivity since the dielectric layer deforms more and the displaced volume is the lower dielectric constant air. This was demonstrated experimentally via indentation depth profiles. For a given applied force, indentation depths were significantly deeper for the porous elastomer film than for the unstructured film.<sup>[67]</sup> Further, increasing the porosity of the material increases the modulus of the material, thus increasing the sensitivity.<sup>[89]</sup>

Using Abaqus FEM simulations, Kim et al. determined that the compressive modulus of porous materials increases as pressure is increased, regardless of pore size, due to the collapse of pores with applied pressure (Figure 3H).<sup>[87]</sup> Interestingly, for a

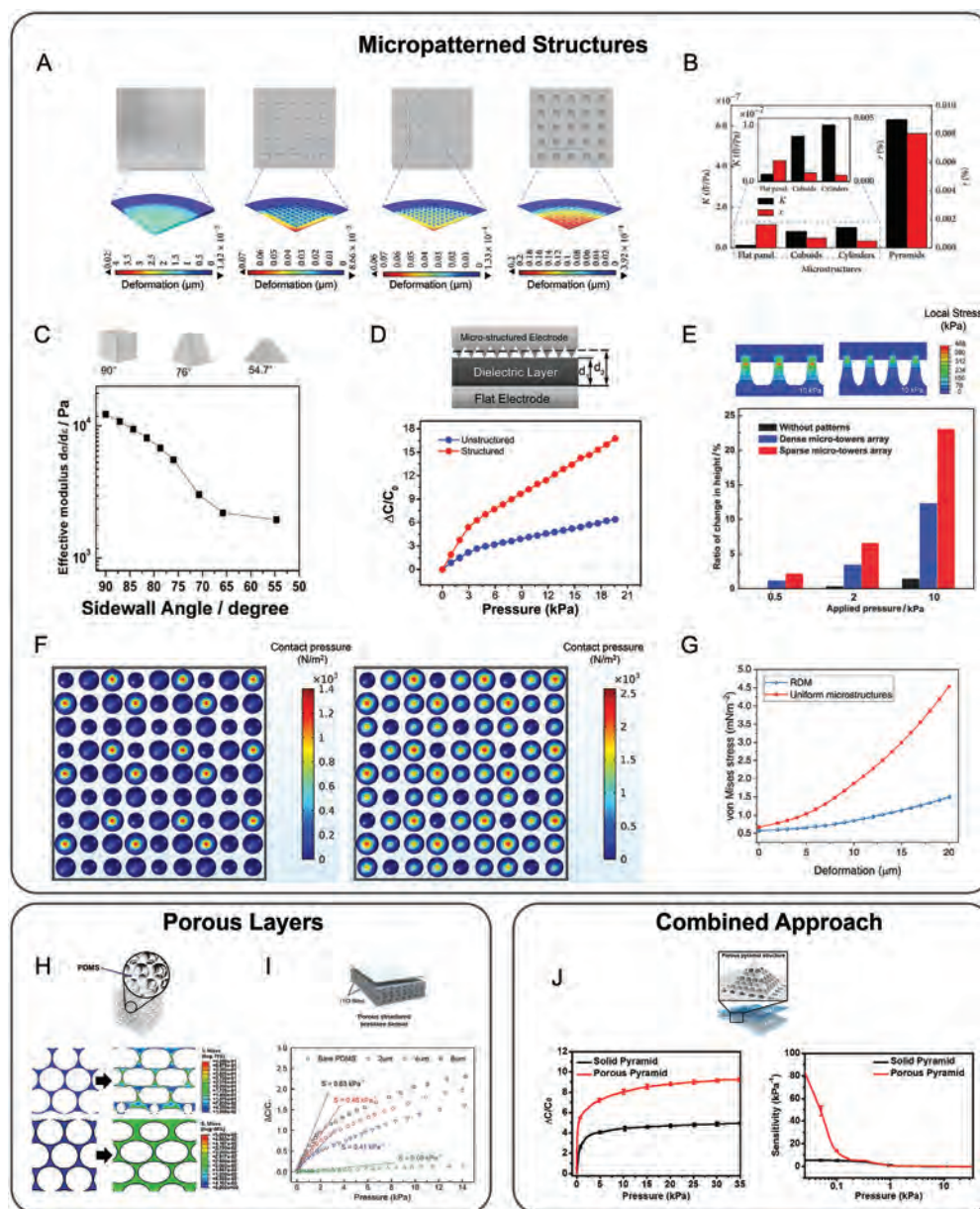


**Figure 3.** Micropatterned structures, porous layers, and combined approaches have been used and tuned to improve performance of capacitive pressure sensors. A) Schematic and deformation of pyramid, cuboid, and cylinder micropatterned structures along with a flat panel or unstructured film for a given applied pressure. Adapted with permission.<sup>[77]</sup> Copyright 2016, Hindawi Publishing Corporation. B) Pyramid microstructures demonstrate highly improved sensitivity compared to unstructured film, cylinder and cuboid micropatterned structures. Here,  $K$  is the sensitivity and  $r$  is nonlinear error. Reproduced with permission.<sup>[77]</sup> Copyright 2016, Hindawi Publishing Corporation. C) Sidewall angle of the microstructures can significantly tune the effective modulus of a material, and in turn tune the sensitivity. Adapted with permission.<sup>[77]</sup> Copyright 2014, Wiley-VCH. D) Side-view of a pressure sensor with a microstructured electrode. The structured electrode (Figure 4E,F) shows a higher sensitivity in both pressure regimes as compared to an unstructured electrode. Adapted with permission.<sup>[84]</sup> Copyright 2018, Wiley-VCH. E) When comparing the stress distributions of sparse and densely packed microtowers, as analyzed by finite element simulations, sparsely packed microtowers show a greater deformation for a given applied pressure. Adapted with permission.<sup>[85]</sup> Copyright 2018, Wiley-VCH. F) Finite element modeling of von Mises stress distribution of randomly dispersed microstructures (RDMs) at different compression levels with five different asperity heights. Adapted with permission.<sup>[86]</sup> Copyright 2018, American Chemical Society. G) The slower rate of change in stress of RDMs (Figure 4C) indicates that the pressure required to deform the RDMs is less than that of uniformly distributed microstructures, contributing to its higher sensitivity. Adapted with permission.<sup>[86]</sup> Copyright 2018, American Chemical Society. H) Simulation of strain responses of microporous materials (Figure 4I) with 500  $\mu\text{m}$  (top) and 250  $\mu\text{m}$  (bottom) diameter pores to applied stress show that the larger pores collapse due to buckling at lower pressures. Adapted with permission.<sup>[87]</sup> Copyright 2018, American Chemical Society. I) Porous dielectric layers of capacitive pressure sensors improve the sensor performance and larger pores further improve the sensor's capacitance change to a given applied pressure. Adapted with permission.<sup>[67]</sup> Copyright 2016, Wiley-VCH. J) Schematic of final device structure of the fabricated capacitive pressure sensor with a porous pyramid structure dielectric layer. Porous pyramid microstructures (Figure 4J,K) demonstrate a greater change in capacitance for a given applied pressure in the low-pressure regime. Porous pyramid microstructures demonstrate a highly improved sensitivity compared to a solid pyramid at low pressures. Adapted with permission.<sup>[75]</sup> Copyright 2018, American Chemical Society.



given fraction of total void space, a material with larger pore sizes will exhibit a lower compressive modulus.<sup>[67,87]</sup> Kim et al. attribute this to the fact that when a porous structure is compressed, the thin columns between the pores undergo buckling. According to Euler, the critical force at which buckling occurs is inversely proportional to the length of the columns between the pores. This buckling process allows the material to compress more for a given applied pressure. Thus, since the columns between larger pores are longer, they will experience buckling at lower applied pressures, deforming more for the given applied pressure, thus leading to a lower compressive modulus.<sup>[87]</sup> On the other hand, the contact between buckled structures may result in hysteresis of the sensors.

Capacitance is in part dependent on the dielectric constant (Equation 1), so change in dielectric constant is also important in dictating the sensitivity of capacitive pressure sensors.<sup>[87]</sup> As pressure is applied to the sensor with a microengineered dielectric, the effective dielectric constant—which accounts for air voids in addition to materials—increases. As the pores begin to collapse upon applied pressure, the ratio of air to elastomer decreases, leading to an increase in the effective dielectric constant, since the elastomer typically has a higher dielectric constant than air. As a result, an increase in sensitivity is observed.<sup>[87]</sup> Thus, larger pore sizes are generally consistent with improved sensitivity for capacitive pressure sensors due to changes in both compressive modulus and permittivity of the dielectric layer.<sup>[67,87]</sup> This was confirmed experimentally by Kang et al. (Figure 3I).<sup>[67]</sup>

Similar to micropatterned structures, porous layers have also been recently used to structure the electrode.<sup>[90]</sup> Using this method, the capacitance change is dependent on the change in contact area between the porous electrode and the dielectric layer.

### 2.1.3. Combined Approach

Further work has demonstrated combining multiple approaches, such as introducing micropores to micropatterns, to help further improve sensitivity.<sup>[75]</sup> Yang et al. found that a porous micropattern resulted in a more compressible dielectric layer, which improved sensitivity compared to solid pyramids

of the same size at low pressures (Figure 3J). Moreover, adding more air voids in the dielectric layer resulted in a greater change in effective permittivity upon compression, which further increased sensitivity.<sup>[75]</sup> As a result, the sensor was highly sensitive below 100 Pa, and could easily detect the landing of a fruit fly with a mass of 0.9 mg.<sup>[75]</sup> However, while a combined approach was found to greatly improve sensitivity at low pressures, the advantages over solid pyramid structures diminished at higher pressures (Figure 3J).<sup>[75]</sup> Thus, it is important to consider the target application for the sensor when choosing a microengineered design.

## 2.2. Performance Comparison

There are many advantages of the different micro-engineering designs. Although it is difficult to compare performance parameters with so many variables changing between methods and designs, some key conclusions can be made (Table 1). First, combining multiple microengineering approaches can significantly improve upon an already effective microengineering strategy. By introducing porous elements to pyramidal microstructures, Yang et al. was able to increase both the limit of detection and the sensitivity of their capacitive pressure sensors as compared to sensors with nonporous pyramids.<sup>[15,75]</sup>

Second, there is often a tradeoff between improved sensitivity and sensor range. In the aforementioned example, the sensing range of Yang et al.'s porous, micropatterned sensor was lower than for its nonporous counterparts.<sup>[15,75]</sup> This is likely due to the saturation of the microstructure at a lower pressure as a result of its improved compressibility. Further, the capacitive pressure sensor with one of the highest sensitivities (44.5 kPa<sup>-1</sup>) also had the lowest range (0–100 Pa).<sup>[75]</sup> The same is true on the other end of the spectrum: the porous structure with the lowest sensitivity of those discussed here (0.86 kPa<sup>-1</sup>) also had the highest range (0–100 kPa).<sup>[87]</sup> As a result, it is critical to decide on performance parameter priorities for the application at hand to determine which design is ideal for a given application.

Third, response times are greatly improved by microengineering because it makes the material more compressible and more elastic.<sup>[15,67,75,76,84,86,87]</sup> This is one of the major advantages of microengineering because it allows for a greater versatility

**Table 1.** Comparison of select capacitive pressure sensor performance based on microengineered features. (NR = not reported).

Authors	Feature	Feature size	Limit of detection	Range of maximum sensitivity	Maximum sensitivity	Response time	Relaxation time
Chhetry et al. <sup>[86]</sup>	Randomly distributed domes	≈26 μm	1.12 Pa	0–1.5 kPa	131.5 kPa <sup>-1</sup>	≈43 ms	≈71 ms
Kang et al. <sup>[67]</sup>	Hierarchical porous structure	2 μm	2.42 Pa	0–1 kPa	0.63 kPa <sup>-1</sup>	40 ms	<1 s
Kim et al. <sup>[75]</sup>	Uniformly sized micropores	≈100 μm	10 Pa	0–100 kPa	0.86 kPa <sup>-1</sup>	<100 ms	NR
Liu et al. <sup>[84]</sup>	Line	≈1 μm	10 Pa	0–3 kPa	1.9 kPa <sup>-1</sup>	<100 ms	<100 ms
Mannsfield et al. <sup>[15]</sup>	Pyramids, lines	6 μm	3 Pa	0–2 kPa	0.55 kPa <sup>-1</sup>	NR	ms range
Wan et al. <sup>[85]</sup>	Microtowers	Diameter: ≈6.5 μm, height: 14 μm	0.8 Pa	0–2 kPa	1.2 kPa <sup>-1</sup>	36 ms	58 ms
Yang, et al. <sup>[76]</sup>	Cylinders	Diameter: 10 μm, height: 5 μm	1 mg	≈0–0.5 kPa	One layer: 3.19 kPa <sup>-1</sup> Two layers: 7.68 kPa <sup>-1</sup>	30 ms	28 ms
Yang et al. <sup>[75]</sup>	Porous pyramids	50 μm	0.14 Pa	0–100 Pa	44.5 kPa <sup>-1</sup>	50 ms	100 ms

of potential applications when limitations of response and relaxation time are eliminated. The same is true for the limit of detection, since improving the compressibility of the electrodes or dielectric layer enables the sensor to compress at a smaller external pressure. This agrees with the sensitivity trend, since sensors with higher sensitivities tend to also have the lowest limits of detection, with few exceptions. If a material is more compressible, it will deform at lower pressures (limit of detection) and will also tend to deform more for a given externally applied pressure (sensitivity).

### 2.3. Fabrication Methods for Geometric Microengineering

There have been several reported examples of fabrication methods used to manipulate the geometry of the electrode or dielectric layer of capacitive pressure sensors. We highlight real microscope images to demonstrate the wide range of structures used in capacitive pressure sensors (Figure 4). In this section, we select reported examples in literature of methods used to microengineer some of these sensors with micropatterned structures, porous layers, and combined approaches.

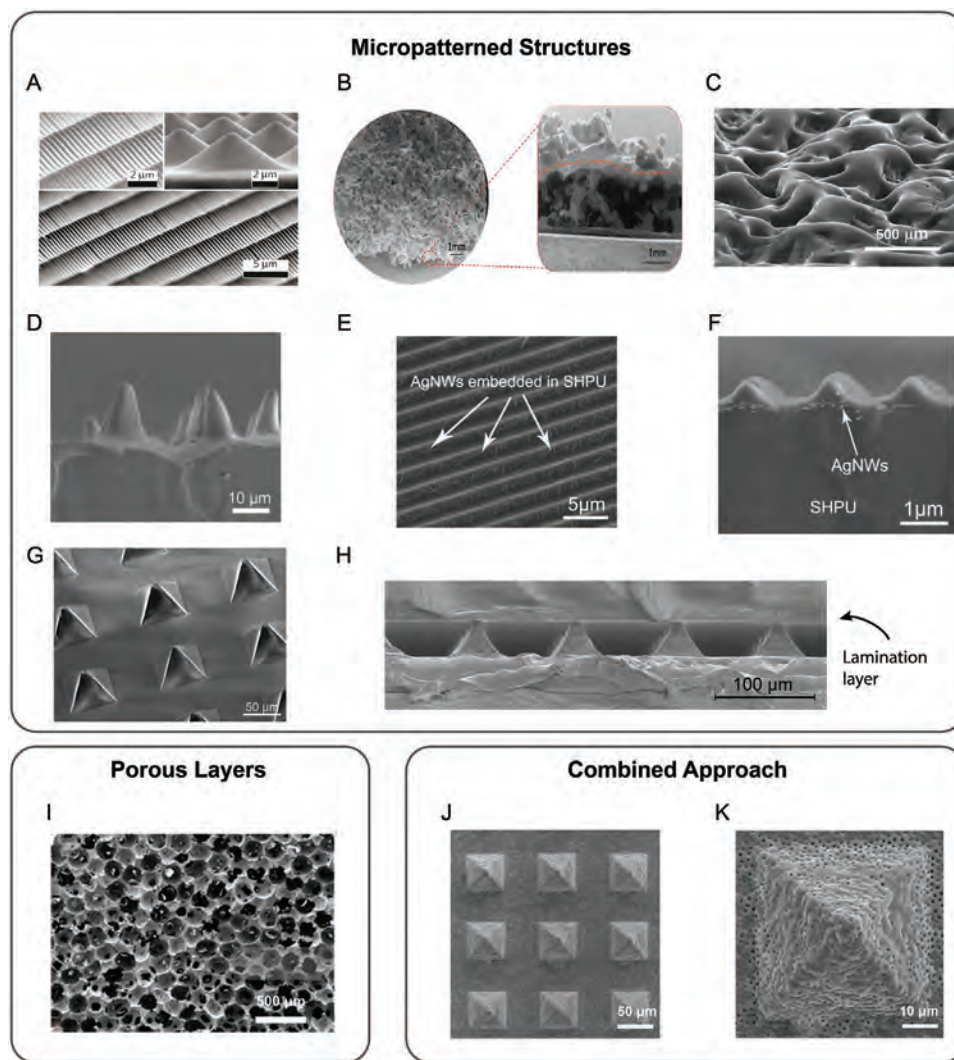


**Figure 4.** Microscope images of fabricated microengineered dielectric layers. A) SEM images of pyramid micropatterned structures made by photolithography. Reproduced with permission.<sup>[15]</sup> Copyright 2010, Macmillan Publishers Ltd. B) *Komochi konbu* structure made using salt and instant sugar. Reproduced with permission.<sup>[93]</sup> Copyright 2019, American Chemical Society. C) FESEM image of Hemispherical-shaped domes fabricated using abrasive paper. Adapted with permission.<sup>[86]</sup> Copyright 2018, American Chemical Society. D) SEM image of the micro-tower structure made using the lotus leaf as a mold. Adapted with permission.<sup>[85]</sup> Copyright 2018, Wiley-VCH. E) Top view SEM image of the line-structured electrode fabricated by plasma treatment of PDMS upon stretching. Adapted with permission.<sup>[84]</sup> Copyright 2018, Wiley-VCH. F) Cross-sectional view SEM image of the line-structured electrode fabricated by plasma treatment of PDMS upon stretching. Adapted with permission.<sup>[84]</sup> Copyright 2018, Wiley-VCH. G) SEM image of pyramid microstructures from a 45° angle. Reproduced with permission.<sup>[71]</sup> Copyright 2019, Wiley-VCH. H) SEM cross-sectional image of the lamination layer and micro-pyramids. Reproduced with permission.<sup>[71]</sup> Copyright 2019, Wiley-VCH. I) SEM image of the microporous material fabricated using DMESA. Adapted with permission.<sup>[87]</sup> Copyright 2018, American Chemical Society. J,K) Top view SEM image of porous pyramid structures made using photolithography-based molds along with polystyrene beads. Reproduced with permission.<sup>[75]</sup> Copyright 2018, American Chemical Society.



### 2.3.1. Micropatterned Structures

Micropatterning the dielectric layer of a capacitive pressure sensor is one of the most common approaches to improving sensor performance. This can be achieved using a wide range of methods such as direct molding from biological or commercial materials or using photolithographic techniques.

One of the most common methods is direct fabrication with a mold, generally using photolithography.<sup>[10,15,17,71,75]</sup> This mold is frequently fabricated from <100> silicon wafers with thermally grown oxide and photolithographic patterning.<sup>[10,15,17,71,75]</sup> First, lithography is used to generate photoresist patterns, followed by an etching of the oxide layer. The remaining oxide layer acts as a mask during the silicon etching process.<sup>[71]</sup> The photolithography etching process can vary depending on the desired mold structure. For example, to make pyramid microstructures, potassium hydroxide is used to etch the silicon wafer due to its nonuniform etching rates, which results in pyramid structures with a sidewall angle of 54.7°. <sup>[17]</sup> Once the etching is complete, the oxide layer can be removed.<sup>[15,17,71]</sup> Afterwards, micropatterned elastomers can be fabricated by dispersing the elastomer onto the mold surface, curing it, and then removing it from the mold (Figure 5A).<sup>[15,17,71]</sup> In order to facilitate removal of the elastomer from the silicon wafer mold, vapor deposition of a fluorinated silane is frequently implemented to create a highly hydrophobic mold surface.<sup>[15,17,71]</sup>

Micropattern molds can also be controllably fabricated from copper.<sup>[76]</sup> Yang et al. used UV lithography to pattern copper foil with rectangular holes. After isotropic wet etching and high temperature melting during chemical vapor deposition, the rectangular holes are reconstructed into an inverse-dome shape, which can be used to mold dome structures.<sup>[76]</sup> Although this fabrication process may be complex, it produces highly reproducible molds.

To circumvent the often-difficult processes required to fabricate molds, there has been increased interest in using readily available materials as molds, including commercially available or biological materials.<sup>[73,74,85,86]</sup> A commonly used commercial material is abrasive paper because it is cost-effective, readily available, and can sometimes be used as a mold without the need for surfactant treatment.<sup>[86]</sup> In this process, the elastomer is simply dispersed on the paper, cured, and then demolded (Figure 4C).

For biological materials, plant leaves, such as the lotus leaf, are commonly used (Figure 4D).<sup>[85]</sup> The lotus leaf is particularly interesting as a natural mold material due to its self-cleaning properties and its hydrophobicity, which makes demolding easier.<sup>[85,91]</sup> The lotus leaf contains microtower structural elements, which can be incorporated into a molded elastomer via soft lithography. In soft lithography, a starting mold is first used to mold an elastomer,<sup>[17,92]</sup> which is then treated to make its surface highly hydrophobic. This elastomer is then used to mold the micropatterned active layer—which, in this example, contains the same microtower structures as the lotus leaf (Figure 5C).<sup>[85]</sup> Although biological and commercially available molds simplify the fabrication process, there is significant variation between molds and nonuniformity within each mold.

Further, simple molds can be made using commercially available materials, such as salt and instant sugar.<sup>[93]</sup> Wang et al.

used this method to design a bionic *komochi konbu* dielectric structure (Figure 4B). To fabricate this structure, they poured a mixture of instant sugar powder, salt grains, and water onto a surface and then dried it to make a template for the PDMS elastomer (Figure 5D). Once the templated elastomer was fully cured on the template, the sugar and salt crystals could be removed by dissolution with the aid of an ultrasonic bath.<sup>[93]</sup> This provides a more cost- and time-effective method of creating a mold for micropatterning, but the mold must be remade for each sample. Moreover, the pattern is less defined than the techniques that employ lithography.

Alternatively, micropatterning can be done by directly structuring the elastomer without using a mold. One way of doing this is to make linear buckled structures by prestraining a cured PDMS film, applying a plasma treatment with low-pressure dry air to generate a silicon oxide layer, and finally releasing the film to form peaks and troughs.<sup>[80,83,84,94]</sup> This can either be used directly as a dielectric layer, can be a template for a micropatterned electrode,<sup>[80]</sup> or can be used as a mold for a micropatterned electrode (Figure 4E,F), making the technique versatile.<sup>[84]</sup> To use it as a template for a micropatterned electrode, Shuai et al. dispersed silver nanowires after the plasma treatment, but before the release of the elastomer substrate.<sup>[80]</sup> The silver nanowires were found to have no effect on the ability to form the buckled structure.<sup>[80,95]</sup> Nevertheless, a downside to not using a mold is the inherent inconsistencies between fabricated sensors.

### 2.3.2. Porous Layers

Introducing a porous structure to the dielectric layer of the capacitive pressure sensors improves its compressibility because it introduces air voids, allowing the structure to more easily deform. Crude methods for fabricating this structure include arranging a material—frequently microspheres—into the desired pore arrangement, pouring and curing an elastomer over the arrangement, and then removing the original material, often by dissolution.

One highly controllable method of achieving porous structures was developed by Kim et al., who used a droplet-based microfluidic-assisted emulsion self-assembly (DMESA) technique to generate uniformly sized spherical micropores over a large area with high spatial uniformity (Figure 4I).<sup>[87]</sup> To fabricate this 3D microstructure, an oil solution containing PDMS and surfactant and an aqueous solution were each prepared and flowed through a capillary tube that met at a T-junction (Figure 6A). This resulted in surfactant-stabilized aqueous droplets in the oil solution. The droplets were then collected in a container, and because water is denser than the oil solution, the droplets sink to the bottom of the container and self-assemble into a closely packed stacked lattice. The PDMS is then allowed to cure while the water evaporates, leaving behind a highly uniform 3D structure. These pores can be tuned from 100 to 500  $\mu\text{m}$  by controlling the relative flow rates of the oil and aqueous solutions, making the sensitivity tunable through this technique.<sup>[87]</sup>

Alternatively, porous structures can be made using stacked microbeads (Figure 6B),<sup>[67]</sup> which can also be used to make

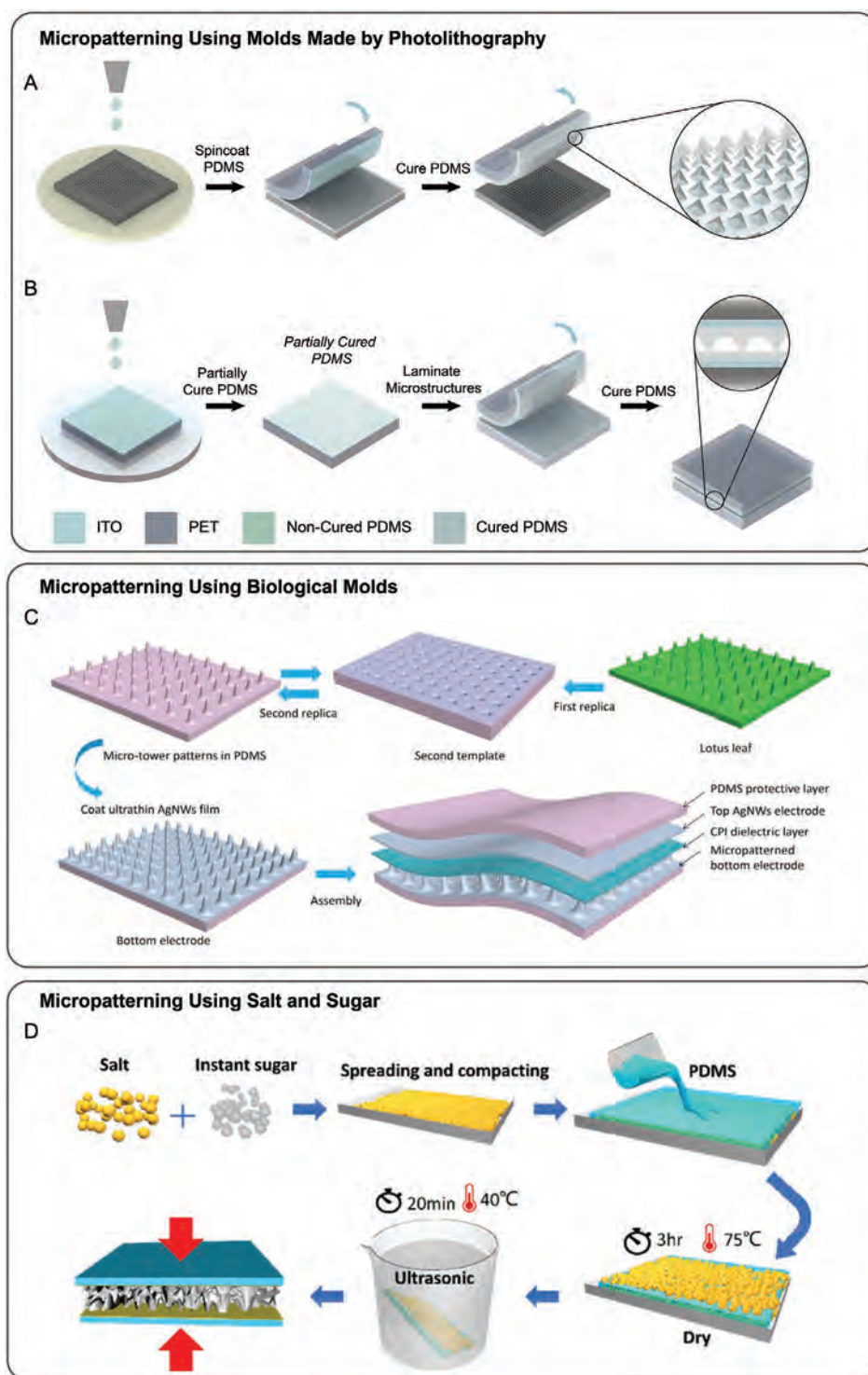


**Figure 5.** Sample schematics of fabrication processes to make micropatterned structures. A) Schematic of a traditional micropatterning method using masks made by photolithography. PDMS is spincoated on the silicon wafer mold. The electrode is placed on the uncured PDMS and allowed to cure. The electrode with the PDMS pyramid pattern (Figure 4G) is removed from the silicon wafer mold. Adapted with permission.<sup>[71]</sup> Copyright 2019, Wiley-VCH. B) PDMS is spincoated on the electrode. PDMS on the electrode is partially cured. The pyramid micropattern is laminated on the partially cured PDMS. The PDMS is allowed to fully cure, to create the final sensor structure (Figure 4H). Adapted with permission.<sup>[71]</sup> Copyright 2019, Wiley-VCH. C) Schematic of a micropatterned structure electrode created using a biological material—lotus leaf—as a mold using soft lithography. The lotus leaf is used to mold a second template, which is then used to mold the final microtower structure (Figure 4D). Reproduced with permission.<sup>[85]</sup> Copyright 2018, Wiley-VCH. D) Schematic of micropatterning using salt and sugar as a dissolvable mold. Salt and sugar are mixed and spread on a surface. The PDMS is poured on top and allowed to cure. Finally, the salt and sugar are removed using an ultrasonic cleaning bath, leaving the micropatterned elastomer (Figure 4B). Reproduced with permission.<sup>[93]</sup> Copyright 2019, American Chemical Society.

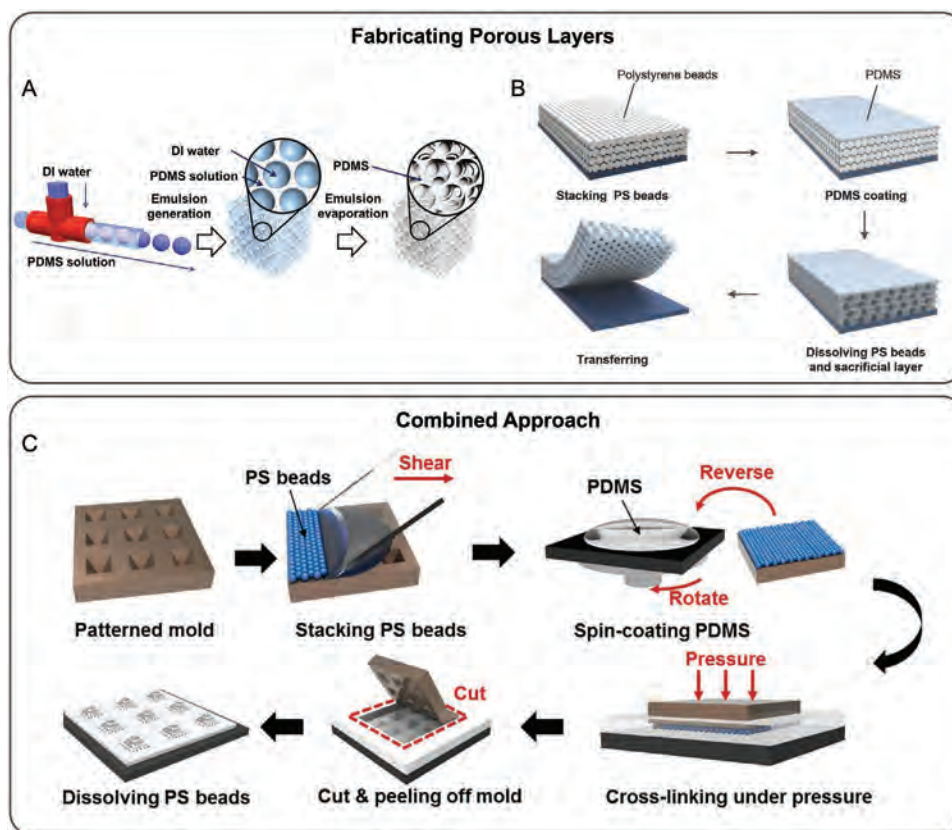


**Figure 6.** Sample schematics of fabrication processes to make porous layers and combined approach structures. A) Schematic of the fabrication process to make 3D microporous structure made using DMESA (Figure 4I). Reproduced with permission.<sup>[67]</sup> Copyright 2018, American Chemical Society. B) Schematic of the fabrication process to make microporous layers using polystyrene beads to create the pores. Polystyrene beads are stacked, coated with PDMS, and then dissolved to make the final porous structure. Adapted with permission.<sup>[67]</sup> Copyright 2016, Wiley-VCH. C) Schematic of the fabrication process of porous pyramid micropatterned structures (Figure 4J,K). Adapted with permission.<sup>[75]</sup> Copyright 2018, American Chemical Society.

highly hierarchical structures. To achieve this, polymer microbeads are stacked on a substrate like silicon using dropcasting. An elastomer film, such as PDMS, can then be coated on the microbeads stacked on the substrate. Once the elastomer cures, the polymer microbeads can be removed, leaving a highly hierarchically structured dielectric layer film.<sup>[67]</sup> The microbead removal process when using polystyrene beads can be done by immersing the sample in an organic solution, providing a porous PDMS layer without significant residue from the polystyrene beads.<sup>[67,96]</sup>

### 2.3.3. Combined Approaches

In order to further improve the performance of pressure sensors, some groups have utilized combined techniques, such as using both molding and porosity introductions (Figure 4J,K).<sup>[75]</sup> Yang et al. developed a porous pyramid micropattern, combining molding and porosity techniques. They began by using photolithography to make a silicon mold with inverse pyramid microstructures (Figure 6C). They then blade coated a solution with polystyrene beads to fill the pyramids with the polystyrene beads. They then placed this on top of a flexible indium tin oxide on poly(ethylene terephthalate) substrate that had spin-cast PDMS that was precured. Pressure and heat were applied

to stack to allow the precured PDMS to penetrate through the spaces between the polystyrene beads and fully cure. The silicon mold was then peeled off, leaving the pyramid microstructure with the polystyrene microbeads still embedded. The microbeads were then dissolved in toluene, leaving behind micropores. Since the microstructures were already mounted on a conductive electrode, one more electrode needed to be applied to the entire structure to create the final structure (Figure 3J).<sup>[75]</sup>

## 2.4. Comparison of Fabrication Methods and Techniques

When choosing a design and fabrication method for a capacitive pressure sensor, several considerations must be taken into account, including ease of fabrication, active layer uniformity, shape and size versatility and uniformity, and scalability. Each of these will vary in importance depending on the specific application, material and equipment availability, and technique expertise.

### 2.4.1. Ease of Fabrication

When weighing the advantages of a given fabrication method, it is important to consider its ease compared to other major



advantages. In literature, fabrication ease is often compared in relation to photolithography, which requires specialized equipment and is considered more costly.<sup>[93,97]</sup> Thus, a process involving lithography to pattern copper or silicon may be costly unless the patterned structures are used as molds, which can be reused many times to replicate structures.<sup>[15,76]</sup> Further, making a porous structure coupled with photolithography adds significant challenges to the fabrication process.<sup>[75]</sup>

Recent work has focused on developing simpler fabrication processes. For example, fabricating a mold using a commercial material such as polystyrene beads, salt, or sugar, may make the fabrication process easier, albeit with less well-defined features.<sup>[67,93]</sup> This is still considered advantageous for many groups because the materials are more accessible and economical. Alternatively, a process such as DMESA, which uses micropores made from oil with PDMS, surfactant, and an aqueous solution, can be used as a moderately simpler fabrication method because it uses fewer specialized equipment, materials, and techniques than photolithography.<sup>[87]</sup>

In addition, recent work has looked at making the microengineering process even simpler by eliminating the need to fabricate a mold. A low level or easy fabrication technique is used to describe a process where the mold is readily available. For example, using a commercially<sup>[86]</sup> or biologically<sup>[85]</sup> available material eliminates the need for mold fabrication or treatment, significantly simplifying the fabrication process. Also, using a process where the elastomer is molded directly, such as using plasma treatment of PDMS, eliminates multiple intensive steps in the fabrication process. However, in some cases, the tunability of the structures may be limited and there may be a large variation of available structures from sample to sample or from batch to batch. These must be taken into account when considering the relevance of a particular design for a desired application, as it may provide an advantage or limitation.

#### 2.4.2. Microengineered Layer Uniformity

As previously discussed, performance of capacitive pressure sensors can be tuned by either microengineering the electrode or the dielectric layer. Uniformity—referring to the distribution and size consistency of the structures and pores—in either of these layers can be critical for particular applications. For example, sensor uniformity is important if the detected pressure is expected to be nonuniform or inconsistent, as this ensures a consistent response regardless of where pressure is applied to the sensor. This could be particularly important for sensors that interface with irregular surfaces like the brain. Nevertheless, uniformity of the microengineered layer often necessitates a more challenging fabrication process, making it an important parameter to consider when choosing a fabrication technique.

High uniformity of the microengineered layer is often achieved using precise and highly controllable fabrication methods to make the mold. This is frequently achieved using photolithography (Figure 4A,G).<sup>[15,17,71,75]</sup> This high uniformity arises from the high uniformity of the photolithography masks, along with the precise etching mechanisms based on chemical reactions with the substrate surface. Further, the flatness of the silicon wafers and the precision of the fabrication process result

in a highly controllable pattern size and distribution, in all three directions, down to the micron scale. However, relatively high uniformity can still be achieved using other methods where one aspect of the structure may be highly uniform while another is more variable. For example, by using a combined approach and fabricating a microporous pyramid structure, Yang et al. achieved a highly uniform pyramid structure with 50  $\mu\text{m}$  base and edge-to-edge lengths from the molds made with photolithography (Figure 4J), but the 2  $\mu\text{m}$  polystyrene spheres created a porous structure with more variability (Figure 4K).<sup>[75]</sup>

Despite the high uniformity of micropatterned structures, uniformity on the device scale may still be difficult to achieve due to the challenge of reproducibly sandwiching structures between the two parallel electrodes when the structures possess only small contact areas between their tips and the opposing electrode. To address this, we recently showed that adding a lamination layer can help anchor micropatterns to the other electrode.<sup>[71]</sup> To do this, a very thin layer of the elastomer is dispersed on the electrode without the micropattern and partially cured. The electrode is then connected to the micropatterns is placed on the other electrode, with the tips anchored in the partially cured elastomer, and then the device is further cured (Figure 5B). This process enabled us to produce highly reproducible pyramid microstructures (Figure 4G,H), which are fully laminated to the other electrode, resulting in a truly parallel plate sensor with highly predictable performance.<sup>[71]</sup>

Moderate uniformity can be achieved by plasma treating the pre-strained elastomer and then releasing the strain to achieve line shapes (Figure 4E,F).<sup>[80,84]</sup> This process results in evenly distributed lines (Figure 4E) with  $\approx 1\ \mu\text{m}$  base width with minor variability (Figure 4F). Although the shape is relatively uniform, control over the uniformity is lower than using a process such as photolithography. Further, when using this as the substrate for the electrode whereby the conductive element is dispersed along the structure, further variability in the structure is introduced due to potential uneven distribution of the conductive element (Figure 4E).<sup>[80]</sup> This also occurs when using a process such as DMESA (Figure 4I) or polystyrene microbead dispersion to achieve the microengineered structure.<sup>[67,87]</sup> This is because the droplets or microbeads are generally uniform in size, but there is less control over their arrangement.

Finally, low uniformity is likely when relying heavily on commercially available<sup>[85,93]</sup> or biological<sup>[86]</sup> materials. First, commercially available materials such as abrasive paper are not intended to be highly uniform in structure, with structures varying in size up to at least 500  $\mu\text{m}$ , and will thus produce a microengineered structure with low uniformity (Figure 4C).<sup>[86]</sup> Alternatively, when using commercially available materials such as salt and sugar to make a mold for the elastomer, low uniformity is likely due to variability in both the arrangement and grain variability (Figure 4B).<sup>[93]</sup> Thus, for such structures, the pressure response may vary more depending on the location of the applied pressure, leading to a large standard deviation for sensor performance and even more variability between sensors. The mold is remade for each sensor, significantly hindering the repeatability of the sensor performance. This may be acceptable for sensors that require a simple detection of pressure, such as detecting a wrist pulse. However, for applications that require quantitative

analysis of the applied pressure, such as strength of airflow or weight of an object, uniformity within the sensor is critical, and alternative fabrication methods should be considered.

#### 2.4.3. Shape and Size Versatility and Tunability

Depending on the fabrication method or mold chosen, there is a different level of control over the versatility and tunability of the shape and size of the microengineered layer of the capacitive pressure sensor. The more control over the structure, the greater the tunability of the sensor's performance parameters, as predicted by our group's experimentally validated model.<sup>[71]</sup> Tunability of the structures and, consequently, the performance parameters are important to be able to make adjustments to a sensor to fit the desired application. For example, changing the size and interstructural spacing of a micropattern can change the initial capacitance, an integral parameter needed to fit to the necessary electronic readout system.<sup>[71]</sup>

When fabricating the mold via a highly controllable process such as photolithography, there is a high level of versatility and tunability in the shapes, sizes, and structures that can be achieved. Photolithography has been used to make a wide range of microstructural shapes, including cylinders, pyramids, and lines.<sup>[15,17,75,76]</sup> The sizes and the interstructural spacings are also easily tunable by changing the photolithography mask design.<sup>[8,17]</sup> Some fabrication techniques, albeit more accessible and high-throughput, only have the capacity to tune size or shape, resulting in a decreased versatility. For example, using DMESA, the micropore sizes can easily be tuned from 100 to 500  $\mu\text{m}$ .<sup>[87]</sup> This is less versatile than photolithography, which has a much wider range between micron-sized structures to hundreds-of-microns-sized structures, but still allows versatility. The interpore spacing, however, is less easily controlled, leading to a decrease in versatility in the fabrication technique, as compared to the patterns made using photolithography. Similarly, using polystyrene microbeads to create the porous structure provides some control over the size of the pores by using polystyrene microbeads with different diameters.<sup>[67]</sup> However, although the average interpore spacing can be varied, due to the stacking technique, there is less control over the inter-pore spacings, limiting the versatility of the fabrication technique.

Finally, microengineering methods using commercial and biological materials can be classified as providing limited versatility and tunability, as only limited sizes and shapes are available.<sup>[85,86]</sup> Similarly, using salt and/or sugar to mold the microengineered layer provides very limited control over the final structure due to the predetermined sizes of the salt and sugar.<sup>[93]</sup> While the spreading of the sugar and salt can be manipulated to tune interstructural spacing, control is limited compared to photolithography techniques or even microbead stacking. Still, if these methods can generate the desired structure with the desired performance characteristics, then tunability may not be as important.

#### 2.4.4. Scalability

Scalability is an increasingly important consideration as research in capacitive pressure sensors progresses toward industrial use.

Scalability can be improved by eliminating steps in the fabrication process, including the need to fabricate a mold, or by using cost-effective and easily attainable materials.<sup>[81,86]</sup> Readily attainable molds and simple designs can also make it easier and more economical to fabricate larger sensors. The materials used to make the molds or the sensors themselves are important for the scalability of the device since readily available materials simplify the fabrication process. When fabricating molds, scalability becomes more attainable when established techniques widespread in industry are adopted, such as photolithography. Further, some works, such as the use of plasma treatment on a pre-strained elastomer to create a line structure, completely eliminate the need for a mold. Finally, the environmental impact of materials may become more important with scale; in that respect, natural materials may be more environmentally friendly and readily available than other alternatives.<sup>[85]</sup>

### 3. Resistive Pressure Sensors

Resistive pressure sensors transduce applied pressure into a change in electrical resistance.<sup>[98,99]</sup> Resistive pressure sensors are governed by the following equation

$$R = \frac{\rho L}{A} \quad (2)$$

where  $R$  is the contact resistance,  $\rho$  is the material's resistivity,  $L$  is the length, and  $A$  is the contact area.<sup>[49]</sup> In general, as a given pressure is applied to the sensor, the resistance decreases. They have been of particular interest due to their simple structure and readout mechanism, similar to capacitive pressure sensors. However, they require constant power consumption and some may be sensitive to temperature.<sup>[34,49]</sup> Further, resistive pressure sensors are generally used due to their wide detection range and long durability.<sup>[100]</sup>

Previously, resistive pressure sensors tended to suffer from low sensitivity, slow response/relaxation speeds, and poor temperature stability, which limit their usability.<sup>[101,102]</sup> These limitations are due to high material modulus, viscoelasticity, and thermal expansion, respectively. The material modulus is important in dictating sensitivity since it defines how much a material will deform for a given applied pressure, with more deformable (low modulus) materials generating a higher change in resistance at a given applied pressure. The viscoelasticity of the material is important in dictating response and relaxation speeds because it determines the speed of the material's response to applied or released pressure. While several strategies have been employed to try to address these limitations, this review will focus specifically on microengineering strategies, including the use of micropatterned structures, porous layers, and multilayered packed structures.<sup>[23,63,103–106]</sup>

Many of the strategies to address sensitivity limitations rely on microengineered structures that cause contact area to increase more with applied pressure than for flat structures (Figure 7A,B). The more a structure can deform to increase the contact area, the higher the sensitivity (Figure 7C,D).<sup>[107]</sup> Since sensitivity is dictated by the change in contact area rather than the change in the distance between the electrodes, as is the case

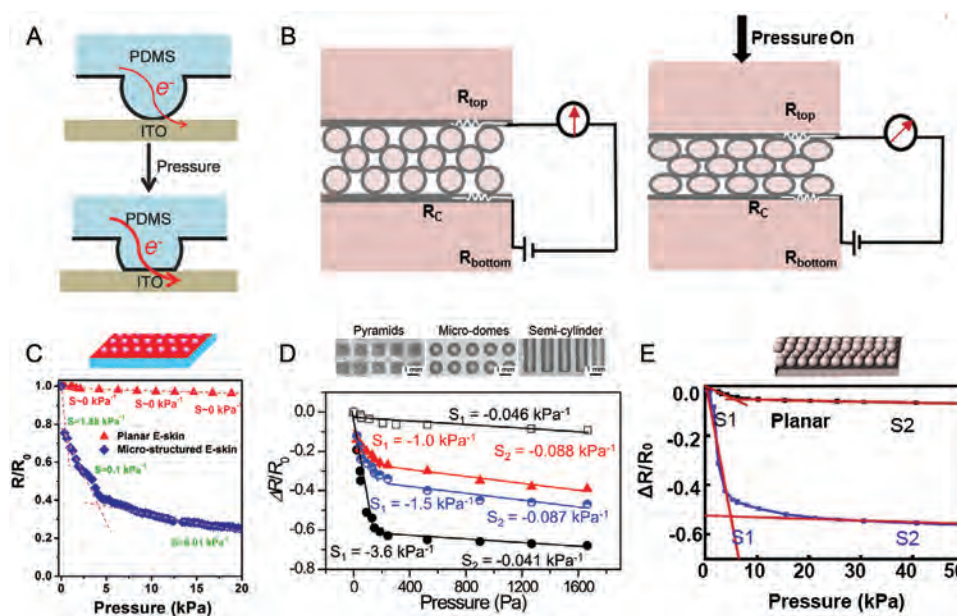


**Figure 7.** Microengineering the active layer in resistive pressure sensors. A) When compressing a micropatterned structure, the contact area increases in all layers and air is displaced. Reproduced with permission.<sup>[97]</sup> Copyright 2018, Wiley-VCH. B) When compressing multilayered packed structures, the contact area increases and air is displaced. Adapted with permission.<sup>[106]</sup> Copyright 2018, Elsevier B.V. C) Microengineered active layers have higher sensitivity than planar or unstructured film. Adapted with permission.<sup>[110]</sup> Copyright 2015, The Royal Society of Chemistry. D) Top view optical image of the micropatterned structures and plot of resistance changes as a function of pressure shows that microengineered structures all have better sensitivity than an unstructured film (from top to bottom: squares, unstructured surface; triangles, pyramid; half solid circles, microdomes; solid circles, semicylinder). Adapted with permission.<sup>[97]</sup> Copyright 2018, Wiley-VCH. E) Microengineered layer shows higher sensitivity than planar or unstructured film. Adapted with permission.<sup>[106]</sup> Copyright 2018, Elsevier B.V.

with capacitive pressure sensors, certain designs may be more advantageous for resistive pressure sensors than capacitive ones. In the following sections, we review microengineering designs for resistive pressure sensors (Section 3.1) and compare their performance parameters (Section 3.2), describe commonly used fabrication methods (Section 3.3), and compare these different approaches in terms of scalability, ease of fabrication, versatility and tunability of the technique, predictability, and uniformity (Section 3.4).

### 3.1. Geometric Microengineering Designs for Resistive Pressure Sensors

#### 3.1.1. Micropatterned Structures

In general, adding air voids to the active layer allows it to deform more easily at a given applied pressure, as air has effectively no resistance to deformation (Figure 7A,B). As previously discussed, micropatterning involves the controlled introduction of micron-sized patterns in the active layer with a variety of potential shapes, of which one of the most common is the pyramid.<sup>[97,108]</sup> As the pyramid deforms, it undergoes structural changes toward a more rectangular shape, which increases its contact area with the electrode.<sup>[17]</sup> The advantage of the pyramid structure is its nonuniform stress distribution, with stress being concentrated at the tip.<sup>[97]</sup> For a given applied pressure, the larger local stress concentrations result in larger changes in contact area compared to non-structured surfaces.<sup>[23]</sup>

Another method to increase sensitivity by increasing the change in contact area upon deformation is to use microdomes.<sup>[23,97,107]</sup> Compared to the pyramid structure, microdomes experience a greater change in contact area for a given applied pressure. When a pyramid with the same base length as the diameter of the microdome was compared, although the experienced stress of the microdome line shape was less for a given applied pressure, the contact area change was larger. As a result, the microdome micropattern is expected to have a higher sensitivity than pyramids of an equivalent size.<sup>[97]</sup>

A third type of micropatterned feature is a micron-scale semicylinder, which exhibits even larger changes in contact area with pressure compared to pyramids and microdomes, as reported by Peng et al. (Figure 8A).<sup>[97]</sup> They analyzed the Von Mises stress field of pressure distribution comparing the three feature types, and found that the stress levels experienced by the pyramid structure were almost an order of magnitude higher than by semicylinder lines, demonstrating that geometry is an important factor for microstructure stress level and, thus, compressibility. However, it is important to note that for resistive pressure sensors, the change in contact area between the active layer and the electrode is more important than the compressibility of the layer. Thus, whereas pyramid micropatterns may be optimal for capacitive sensors, for which sensitivity depends on the deformation of the dielectric layer, they may not be ideal designs for resistive sensors. In fact, Peng et al. found that the rate of increase in contact area of the semi-cylinder lines within the pressure range of 0–2 kPa was significantly higher than the other tested microstructures



at both low and high pressures, explaining its superior sensitivity.<sup>[97]</sup> As the contact area increases with compression, the microstructure tends to saturate, resulting in a decrease in sensitivity at higher pressures.<sup>[97]</sup>

Gao et al. also used finite element modeling (FEM) to compare semicylinders (referred to as “micro-ridges” in their work) and microdomes (Figure 8B–D).<sup>[107]</sup> Surprisingly, they found that microdomes were more sensitive than semicylinder lines, which they attributed to greater stress concentration at the tip of the microdome and therefore greater compressibility. The difference in sensitivity trends observed by Peng and Gao may be due to the difference in the size of their microstructures, with almost two orders of magnitude difference in the diameters of the structures, along with the different interstructural spacing in each work. When structures are large and close together, as is the case in Peng et al.’s work, the compressibility of the microdomes and microcylinders becomes more similar. Thus, what distinguishes the two structures is that the microcylinders have more contact area that can be increased. However, when the structures are smaller and more spread out, they are more compressible, as is the case with the micro-domes in Gao et al.’s work. Thus, it is likely that the greater compressibility of the microdomes under this condition is so much larger than the microcylinder line structure that that is the dominating factor in determining the sensitivity of the sensor. Thus, when choosing how to microengineer the active layer of a sensor, it is important to consider the size and inter-structural spacing of the structures, in addition to their shape.

Another approach to improve sensor performance relies on hierarchically structured micropatterns (Figure 9A–C).<sup>[24,109–111]</sup> Shi et al. used FEM to show that the hierarchical structure of the papillae of lotus leaves causes a large increase in contact area with applied pressure (Figure 8E).<sup>[109]</sup> To simplify its complicated structure for modeling purposes, they treated the papillae as simple hemispheres with neo-Hookean elasticity—similar to microdomes—but with a hierarchical structure comprising nanodomes on the hemispheres (Figure 8E). Further, they modeled the interactions between individual elements in the micropattern, which complicates the analysis but improves the accuracy of the model. The importance of the hierarchical structure was highlighted by comparing microdomes with nanodomes to ones without. Whereas the contact area quickly saturates with applied pressure for structures without nanodomes, the hierarchically structured domes enable a more steady and continuous increase in contact area with pressure, so that they exhibit both higher sensitivity and larger linear range compared to the same structure with a smooth surface.<sup>[109]</sup>

When modeling these structures, it is important to note that the modeling can easily become more complicated. For example, Pang et al. used finite element analysis to compare elastomers molded using abrasive paper to more traditional micropatterned single layers, such as pyramids, microdomes, and microtowers (Figure 8F).<sup>[103]</sup> They modeled the elastomer as randomly distributed spinosum (a layer of the epidermis), which, although a more complicated model, allowed them to better understand the advantage of this nonuniform structure because they were able to see that stress is concentrated at the initial contact peak and results in large changes in contact area as a result. When translating this information into the change in contact area, and consequently the relative change in resistance as a function of pressure, it was

clear that the randomly distributed spinosum (RDS) performed the best within the analyzed pressure range (Figure 8F).<sup>[103]</sup> It is important to note that this was compared to one specific configuration of a uniformly arranged micropattern, so results may be different for structures of different sizes and distribution.

Despite the information that can be gleaned from the aforementioned models, it is important to note that simplifications are often made to more easily simulate the changes in the microstructures with applied pressure, which increases the degree of uncertainty when it comes to performance predictability. To ensure that a proposed design will work for its intended application, it is therefore important to experimentally validate these computational predictions when possible.

### 3.1.2. Porous Layers

An alternative method of microengineering the active layer of resistive pressure sensors to improve performance is to introduce micropores.<sup>[44,87,112–114]</sup> Using FEM to simulate samples with different pore sizes, Kim et al. found that modulus changes based on pore size and pore density.<sup>[87]</sup> Further, Visser et al. found that modulus changes whether the overall structure is open-cell or closed-cell (Figure 9A).<sup>[112]</sup> An open-cell foam refers to a structure that has a continuous gas phase with solid structures intervening, which means that fluids can easily flow through the material. By contrast, a closed-cell foam has discrete bubbles with surrounding cell walls so that fluids cannot flow freely through the structure, but they can generally withstand greater loads.<sup>[112]</sup> As with capacitive pressure sensors, the modulus of the active layer directly affects the sensitivity of the sensor, so larger pore sizes that cause the active layer to have a lower effective modulus have larger sensitivities than their small pore size counterparts (Figure 9B).<sup>[87]</sup> However, it is important to note that since the active layer becomes more deformable with larger pores, the dynamic range of the highest sensitivity design may be smaller than that of sensors with smaller pores, since they will increase in effective compressive modulus at lower pressures.

### 3.1.3. Multilayered Packed Structures

Multilayered packed structures are also used to improve sensor performance.<sup>[106,110,115]</sup> Modeling these structures requires a thorough analysis of how contact area changes with pressure based on stress distributions both between structures (Figure 9C,D) and between the structures and the electrodes (Figure 9C).<sup>[106,110]</sup> For example, resistive sensors can be fabricated by layering carbon nanotube-wrapped polydimethylsiloxane (PDMS) microspheres, as analyzed by Xu et al. (Figure 9C).<sup>[106]</sup> Since there are multiple layers of microspheres in such a structure, they needed to account both for the interactions between the microspheres themselves and between the microspheres and the flat electrodes, which are both affected by applied pressures.<sup>[106]</sup> Using FEM, they found that local stress at both types of contact points increases with increasing pressure. Thus, when an external pressure is applied, the resistance decreases due to an overall decline in contact resistance of the device from the increase in contact area between the conductive

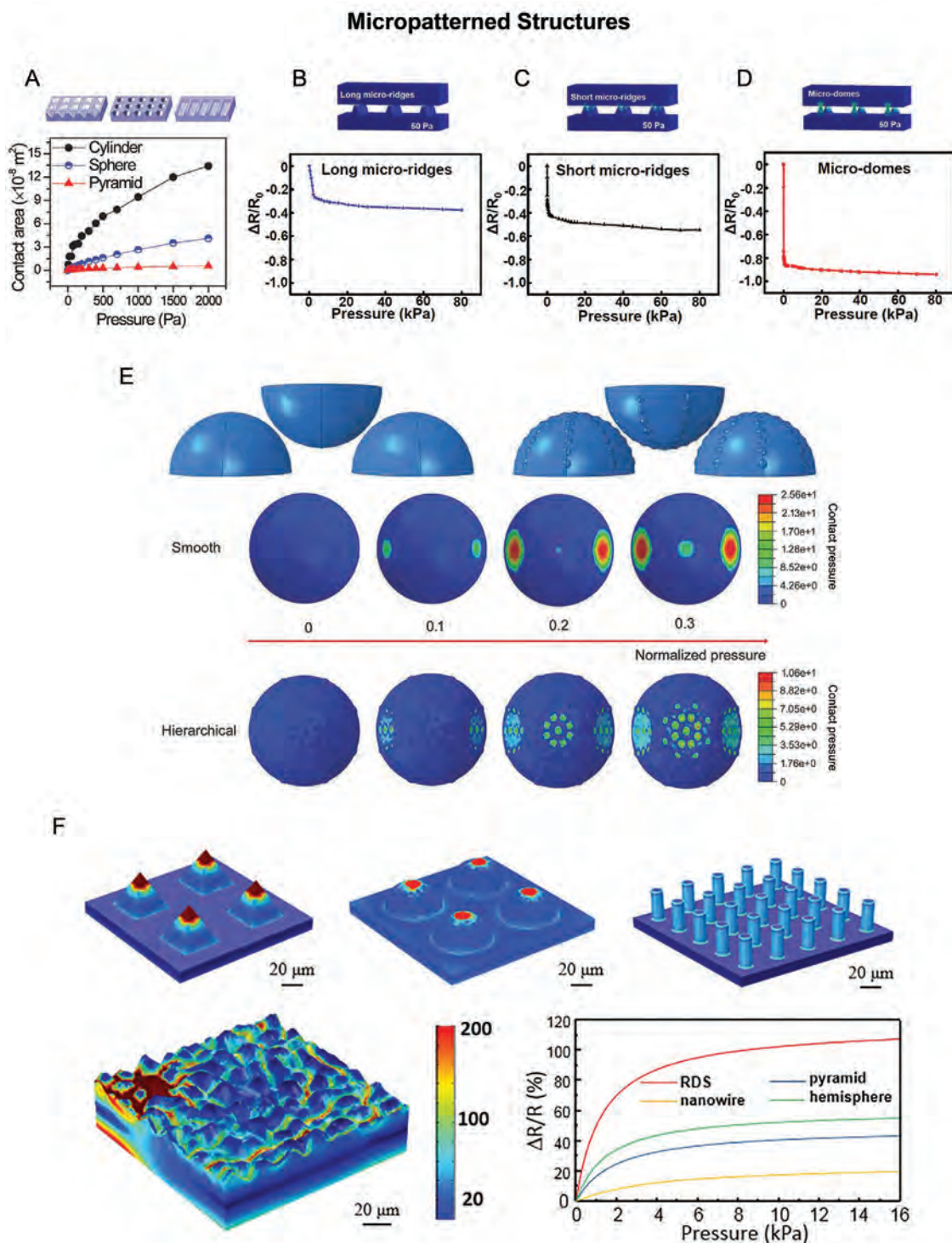


**Figure 8.** Advantages and tunability of micropatterned structures in resistive sensors. A) Finite element modeling of micropatterned structures of domes (spheres, Figure 10B), semicylinders (Figure 10C), and pyramids (Figure 10A) show that cylinders have the greatest change in contact area. Adapted with permission.<sup>[97]</sup> Copyright 2018, Wiley-VCH. B–D) When experimentally comparing long microridges (semicylinders,  $\approx 1000\ \mu\text{m}$  in length, Figure 10B), short microridges ( $\approx 100\ \mu\text{m}$  in length, Figure 10E), and microdomes (Figure 10F), microdomes were found to have the greatest change in resistance at low pressures. Adapted with permission.<sup>[107]</sup> Copyright 2019, IOP Publishing Ltd. E) Finite element modeling of the contact pressure distribution of nanostructured micropatterned structures (hierarchical) as compared with smooth structures. Illustration of a smooth (top left) and hierarchical (top right) contact areas. Adapted with permission.<sup>[109]</sup> Copyright 2018, Wiley-VCH. F) Finite element modeling comparing pressure distributions of various micropatterned structures—pyramids, domes (hemispheres), towers (nanowires), and random distribution spinosum (RDS)—with 5 kPa applied. The results of the modeling were translated into curves of resistance change as a function of pressure, demonstrating the RDS has the highest change in resistance at low pressures. Reproduced with permission.<sup>[103]</sup> Copyright 2018, American Chemical Society.

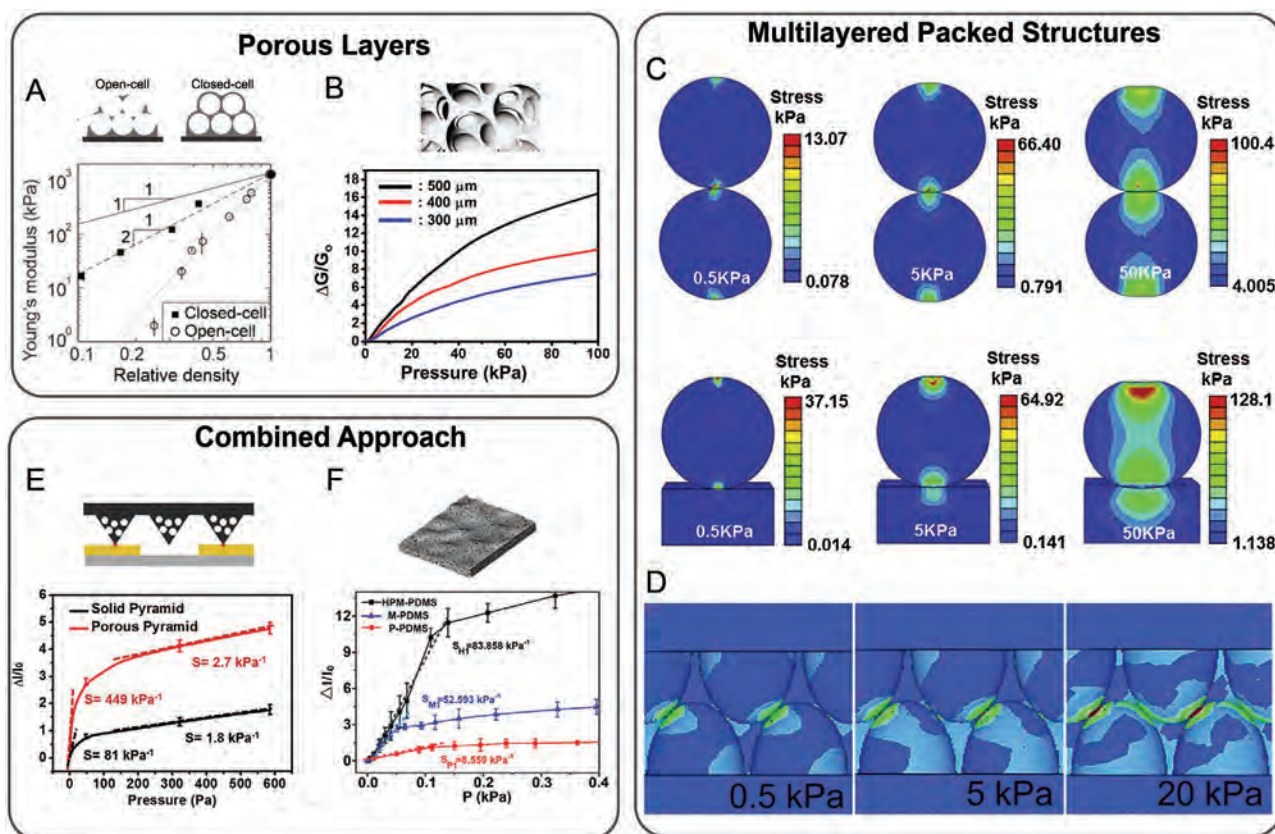


**Figure 9.** Tunability of porous layers, multilayered packed structures, and combined approaches for resistive sensors. A) Young's modulus of the porous layers as a function of the relative density of the micropores (Figure 11E,F). Adapted with permission.<sup>[112]</sup> Copyright 2019, Wiley-VCH. B) The plot of relative conductance change as a function of pressure for varied pore sizes (Figure 11C,D) demonstrates that performance is dependent on pore size. Adapted with permission.<sup>[87]</sup> Copyright 2018, American Chemical Society. C) Finite element analysis of the stress distribution between spheres and between spheres and flat electrode as they are being compressed at 0.5, 5.0, and 50 kPa, respectively. Adapted with permission.<sup>[106]</sup> Copyright 2018, Elsevier B.V. D) Finite element modeling showing stress distribution of multilayered micro-papillae with applied pressure. Adapted with permission.<sup>[110]</sup> Copyright 2015, The Royal Society of Chemistry. E) The plot of relative change in current as a function of pressure demonstrates that porous pyramid (Figure 4),K) shows better performance than solid pyramids at low pressures. Adapted with permission.<sup>[75]</sup> Copyright 2018, American Chemical Society. F) The plot of change in current as a function of pressure for hybrid porous microstructure (HPM-PDMS, Figure 11J,K), microstructured/micropatterned (M-PDMS), and porous (P-PDMS) microengineered active layers highlights an advantage of using a combined approach of HPM-PDMS. Adapted with permission.<sup>[63]</sup> Copyright 2019, American Chemical Society.

spheres. The higher the increase in contact area, the more the resistance will decrease for a given applied pressure.<sup>[106]</sup>

Similarly, Wei et al. used FEM to understand the change in the contact area between two layers of rose petal micro-papillae arrays that are facing each other (Figure 9D).<sup>[110]</sup> To reduce modeling complexity, they simplified the papillae geometry into ellipsoids and estimated a density of the micro-papillae to computationally model interactions between structures.<sup>[110]</sup> They found that stress is concentrated at contact spots between micropapillae, so that higher structure densities resulted in a larger amount of contact spots where stress will concentrate.<sup>[110]</sup> This analysis explains why this multilayered structure performs well as a resistive pressure sensor.

### 3.1.4. Combined Approach

Lastly, combining two or more of the aforementioned approaches has been used to further improve sensor

performance. For example, the porous pyramids used in capacitive pressure sensors can be used in resistive sensors by grafting conductive polypyrrole onto the structures (Figure 9E).<sup>[75]</sup> As with capacitive sensors, Yang et al. found that making the pyramids porous greatly improved sensitivity at low pressures, but in this case the improvement was due to an increase in the contact area with the electrode upon deformation and within the porous pyramid structure. In a similar approach, a hybrid porous microstructure was made by micropatterning a porous material.<sup>[63]</sup> Here, it was found that the hybrid porous microstructure resulted in a much higher sensitivity than a sensor with only micropatterning or only porous materials (Figure 9F). In these examples, not only do the additional air voids increase compressibility of the material, but they also add more potential contact points, significantly increasing sensitivity.

In another example, hollow spherical shells are introduced to allow an inherently brittle nanostructured material to have a tunable effective modulus that is capable of withstanding large effective stresses and strains.<sup>[104,116]</sup> Thus, the introduced



air is used to make an inherently brittle material more elastic. Compared with other hollow-structured materials, these have structures in the tens of microns range and are sensitive at lower pressure regimes, likely because of the smaller structures.<sup>[104]</sup> These nanocrystalline materials were made into hollow sphere geometries and can withstand extremely high compression before failing and extremely high shear stresses relative to their ideal strength. By increasing the thickness of the shell, the stiffness of the shells increases. Further, the hollow sphere-based sensor demonstrated performance independent of temperature, a major challenge of resistive pressure sensors.<sup>[104]</sup> Thus, spherical shells can be used to improve the performance of a sensor with a brittle active layer to make it more elastic while maintaining its high modulus and temperature-independence.<sup>[104]</sup>

### 3.2. Performance Comparison

Once we identify the advantages of each of the different micro-engineering designs, it is important to then compare the effects of each on the performances of resistive pressure sensors (Table 2). For the sake of comparison, we will refer to the absolute values of reported sensitivities; depending on their definition of sensitivity, some authors report negative values and others report positive ones. In the traditional definition for sensitivity for a resistive sensor, which is the relative change in resistance divided by pressure (Equation 3), values are negative since resistance decreases with pressure.

$$S = \frac{\Delta R/R_0}{P} \quad (3)$$

However, if the authors define the sensitivity based on the difference between the higher and lower resistance values, the

sensitivity will be positive. Alternatively, if the authors define sensitivity based on the change in current, then sensitivity values will also be positive, since current flow with applied voltage is inversely related to resistance.

As with capacitive pressure sensors, it is difficult to identify intricate effects of each of the microengineered structures due to the wide range of variables between each of the highlighted structures. However, some general conclusions can still be drawn. First, when comparing sponges or porous structures, it is clear that larger pores in a given volume of active layer results in a higher sensitivity.<sup>[87,117,118]</sup> This is likely due to the increased compressibility of the sponges with larger pores relative to the skeleton, as previously discussed for capacitive pressure sensors.<sup>[67,87]</sup> In this case, the increased compressibility is accompanied by increase in the contact area for a given external pressure, which will improve its sensitivity.

Second, compared to capacitive pressure sensors, there seems to be less of a clear relationship between the range and sensitivity of resistive pressure sensors. This difference is likely due to the fact that capacitive pressure sensor performance is highly dictated by the compressibility of the dielectric material, while resistive pressure sensors are dependent on the change in active layer contact area. Depending on the structure, contact area can still increase significantly even when the compressibility of the active layer decreases, which would extend the high sensitivity pressure range. With this in mind, the three sensors discussed that have the highest sensitivities (above 100 kPa<sup>-1</sup>) also have the lowest range for that sensitivity (well below 1 kPa).<sup>[75,104,119]</sup> These are important considerations when looking to address a specific need to ensure that both the required sensitivity and pressure range are achievable with a given design.

**Table 2.** Comparison of select resistive pressure sensor performance based on microengineered features. (NR = not reported).

Authors	Feature	Feature size	Limit of detection	Range	Sensitivity	Response time	Relaxation/recovery time
Gao et al. <sup>[107]</sup>	Long microridges, short microridges, microdomes	18 μm	1 Pa	5 Pa–2 kPa	1.82 kPa <sup>-1</sup>	0.036 s	0.052 s
Ge, et al. <sup>[117]</sup>	Sponge	≈100 μm	NR	0–3.24 kPa	0.152 kPa <sup>-1</sup>	96 ms	NR
Jia, et al. <sup>[119]</sup>	Skin-like wrinkles	NR	42 Pa	100–200 Pa	178 kPa <sup>-1</sup>	261 ms	131 ms
Pan, et al. <sup>[104]</sup>	Hollow spheres in lines	lines: 1 mm, spheres: ≈1 μm	<1 Pa	0–30 Pa	56.0–133.1 kPa <sup>-1</sup>	47 ms	≈50 ms
Pang et al. <sup>[103]</sup>	Spinousum	NR	16 Pa	0–2.6 kPa	25.1 kPa <sup>-1</sup>	120 ms	80 ms
Peng et al. <sup>[97]</sup>	Pyramids, microdomes, semicylinders	1 mm	1 Pa	0–200 Pa	3.6 kPa <sup>-1</sup>	30 ms	50 ms
Shi et al. <sup>[109]</sup>	Papillae	≈15–20 μm	5 Pa	0–25 kPa	1.2 kPa <sup>-1</sup>	NR	NR
Tewari, et al. <sup>[118]</sup>	Foam	skeleton ≈100 μm, pores ≈ μm size	3.7 Pa	0–2.7 kPa	0.022 kPa <sup>-1</sup>	30 ms	NR
Wei et al. <sup>[110]</sup>	Papillae	≈20 μm	<2 Pa	0–2 kPa	1.35 kPa <sup>-1</sup>	36 ms	30 ms
Xu et al. <sup>[106]</sup>	Spheres	<100 μm	0.02 kPa	0–1 kPa	0.111 kPa <sup>-1</sup>	≈0.1 s	0.15 s
Yang et al. <sup>[75]</sup>	Porous pyramids	50 μm	0.14 Pa	0–10 Pa	449 kPa <sup>-1</sup>	9 ms	30 ms
Wang et al. <sup>[115]</sup>	Stacked microdomes	≈2.5 μm	0.5 Pa	0–10 kPa	196 kPa <sup>-1</sup>	<26 ms	NR
Yu et al. <sup>[23]</sup>	Lines	≈20 μm	7 Pa	0–1 kPa	0.101 kPa <sup>-1</sup>	10 ms	15 ms
Zhao et al. <sup>[63]</sup>	Micropatterned porous material	height ≈ 2.5 μm, length ≈ 58.2 μm	0.5 Pa	0–140 Pa	83.858 kPa <sup>-1</sup>	170 ms	190 ms
Zhong et al. <sup>[121]</sup>	Clavate groove-shaped	18 μm	<1.6 Pa	0–2.76 kPa	19.4 kPa <sup>-1</sup>	30 ms	42 ms

Third, as was the case with capacitive pressure sensors, microengineering the active layer of resistive pressure sensors plays an integral role in improving response and relaxation times. In all cases, this is due to the increase in air voids in the active layer, which makes the layer not only more easily deformed, but also aids in its recovery. For many applications, such as tracking of blood pressure in the human body, response and relaxation times may be the limiting factors for pressure sensors, so using microengineering in these cases is critical. Microengineering the active layer also generally improves the limit of detection. This is simply due to the fact that the increased compressibility of the active layer enables it to respond to smaller loads.

Finally, it is important to note that there does not seem to be a clear optimal design for resistive pressure sensors that best improves all performance parameters, likely due to the grave differences in feature sizes, interfeature spacing, materials used, and other relevant parameters among reported sensors. This implies that a wide range of design options is available for different applications, and careful consideration of both performance and fabrication needs must be taken into account.

### 3.3. Fabrication Methods for Geometric Microengineering

Several fabrication methods have been reported to manipulate the geometry of the active layer of resistive pressure sensors. We highlight real microscope images to demonstrate the wide range of structures used in resistive pressure sensors (Figures 10 and 11). In this section, we report selected examples in literature of some of these methods used to microengineer sensors with micropatterned structures, porous layers, multi-layered packed structures, or a combined approach.

#### 3.3.1. Micropatterned Structures

Most of the approaches used to make micropatterned structures for resistive sensors involve initially patterning an elastomer using methods similar to those used for micropatterning the dielectrics in capacitive pressure sensors. However, since resistive sensors rely on a change in electrical resistance upon deformation, additional steps must be taken to render the active layer at least partially conductive. Reported methods of introducing conductive elements into the patterned elastomer can be grouped into two categories: coating the structure or directly integrating the conductive element into the elastomer. In the following section, we briefly illustrate examples of how elastomers have been micropatterned to make resistive sensors, analogous to fabricating capacitive sensors, with a key distinction being the additional strategies used to incorporate electrical functionality into these elastomers either before or after patterning.

To generate micropatterned elastomers, most approaches can be classified as either using a mold to make the final structure or directly patterning the active layer (Figures 10 and 12). In the former case, a mold is used to either directly or indirectly shape a material, often an elastomer.<sup>[15,75–77,111]</sup> The various methods for making molds discussed in the capacitive sensors section (Section 2.3), including photolithography, apply for

making resistive sensors as well. In addition, Peng et al. used 3D printing along with soft lithography to create a mold for the desired micropatterns (microdomes, microcylinders, and pyramids) for their resistive sensors, though they were only able to produce 1000  $\mu\text{m}$  structures (Figure 10A–C). Subsequently, carbon nanofibers were spray coated onto the micropatterned films to impart piezoresistive capabilities.

As with capacitive pressure sensors, there has also been increased interest in using already-made materials as molds to avoid the often lengthy and intensive processes required to create the mold. One popular approach has been to use natural materials as molds, including leaves of different plants, such as the lotus or rose (Figure 10G–I).<sup>[105,109,110]</sup> To coat the structures directly molded from a rose petal template, Guo et al. used “polymer-assisted metal deposition” (PAMD), enabling a low-cost fabrication that can be used industrially for roll-to-roll processing (Figure 10G).<sup>[105,120]</sup> To generate the metallic coating, poly[2-(methacryloyloxy)ethyl-trimethylammonium chloride] (PMETAC) was first grafted onto the elastomer surface, followed by an immersion in an aqueous  $(\text{NH}_4)_2\text{PtCl}_4$  solution in order to immobilize the ionic species  $[\text{PtCl}_4]^{2-}$  onto the quaternary ammonium groups in the PMETAC. The substrate was then rinsed with deionized water and immersed in an electroless deposition bath of copper to form a thin layer of copper on the structured surface.<sup>[105]</sup>

Despite their prevalence, variability among natural molds may restrict their use in applications that require a high degree of reproducibility. To address this, the same leaf mold can be used to make the inverse impression by first creating a mold from polyvinyl alcohol that would give the inverse of the leaf structure, and then using that as the mold for the sensor (Figure 12A).<sup>[110]</sup> This would result in the microstructure in the sensor to be identical to that of the rose leaf mold itself (Figure 10H). Using this approach, a simple method for fabricating resistive sensors was performed by drop-coating a copper–silver suspension onto the mold followed by drop-coating of the PDMS elastomer. The system was cured and then peeled off, resulting in the structured composite elastomer.<sup>[110]</sup>

Another method employed to take advantage of premade materials is the use of commercial molds. Pang et al. used abrasive paper to mold PDMS, which resulted in an interconnected web-like network (Figure 12D).<sup>[103]</sup> The micropatterned template was then dip-coated with conductive material, allowing more connections between the conductive parts when a pressure is applied.<sup>[103]</sup> An alternative commercially available product that has been used to mold the elastomeric material is nylon textile.<sup>[121]</sup> Distinct from the previous method, instead of using the molded elastomer as a template for surface coating, Zhong et al. dispersed silver nanowires in the elastomer prior to molding.<sup>[121]</sup> This allows for interpenetrating conductive material in the elastomer, which means that as pressure is applied, there will be more contact points between conductive species, causing a more dramatic resistance change in the material. Further, this process does not require manipulation to ensure adherence of the conductive layer to the elastomer, as is the case with PAMD.

As opposed to using a mold to replicate a micropattern, other groups have chosen to directly pattern their elastomeric layer.<sup>[23,107,119]</sup> One method of doing this is by directly

## Micropatterned Structures

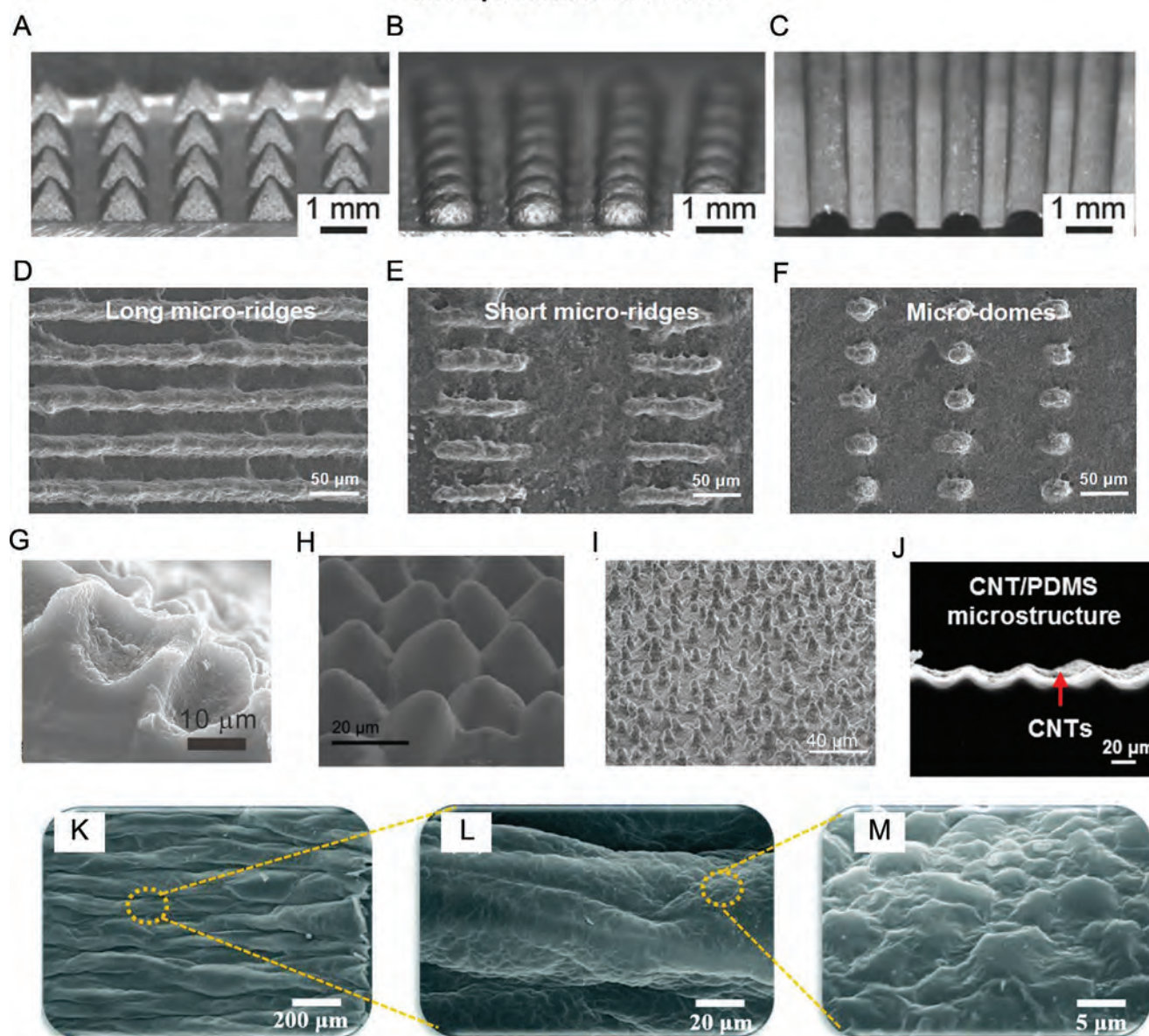


**Figure 10.** Microscope images of fabricated micropatterned structures. A–C) Side view optical images of pyramids, microdomes, semicylinder lines, respectively, fabricated using molds made by 3D printing. Reproduced with permission.<sup>[97]</sup> Copyright 2018, Wiley-VCH. D–F) Top-view SEM images of long microridges/semicylinder lines, short microridges, and microdomes, respectively, made by directly laser microengineering the elastomer. Adapted with permission.<sup>[107]</sup> Copyright 2019, IOP Publishing Ltd. G) Cross-sectional SEM image of the inverted leaf micropatterns molded from a rose petal. Adapted with permission.<sup>[105]</sup> Copyright 2015, Wiley-VCH. H) 45° view SEM image of papillae micropatterned PDMS made from a rose petal mold. Adapted with permission.<sup>[110]</sup> Copyright 2015, The Royal Society of Chemistry. I) SEM image of the lotus leaf papillae. Scale bar: 40 μm. Adapted with permission.<sup>[109]</sup> Copyright 2018, Wiley-VCH. J) SEM image of the wrinkled structure made using UV/O<sub>3</sub> treatment upon stretching of PDMS. Adapted with permission.<sup>[23]</sup> Copyright 2018, IOP Publishing Ltd. K–M) SEM images of the wrinkled morphology fabricated using chemical treatment upon stretching of an elastomer. Adapted with permission.<sup>[119]</sup> Copyright 2019, The Royal Society of Chemistry.

laser micropatterning the desired structure onto a cured elastomeric layer, followed by drop-coating a carbon nanotube solution to coat the patterned structures. Doing so allows for a relatively controllable, well-defined structure while maintaining time-efficiency and scalability.<sup>[107]</sup> This technique was used to make microdomes and cylindrical microridges; however, realizing tapered shapes, such as pyramids, may be challenging (Figure 10D–F). While this method is not as precise as

photolithography and requires a highly precise laser to achieve well-defined features, it has the advantage of requiring fewer steps in the fabrication process.

The elastomeric layer can also be directly micropatterned by applying mechanical strain. For example, Yu et al. molded PDMS by prestraining the cured elastomer and exposing it to a flood exposure of UV light (Figure 10J).<sup>[23]</sup> Upon release of strain, linear or wrinkled micropatterns were formed on the



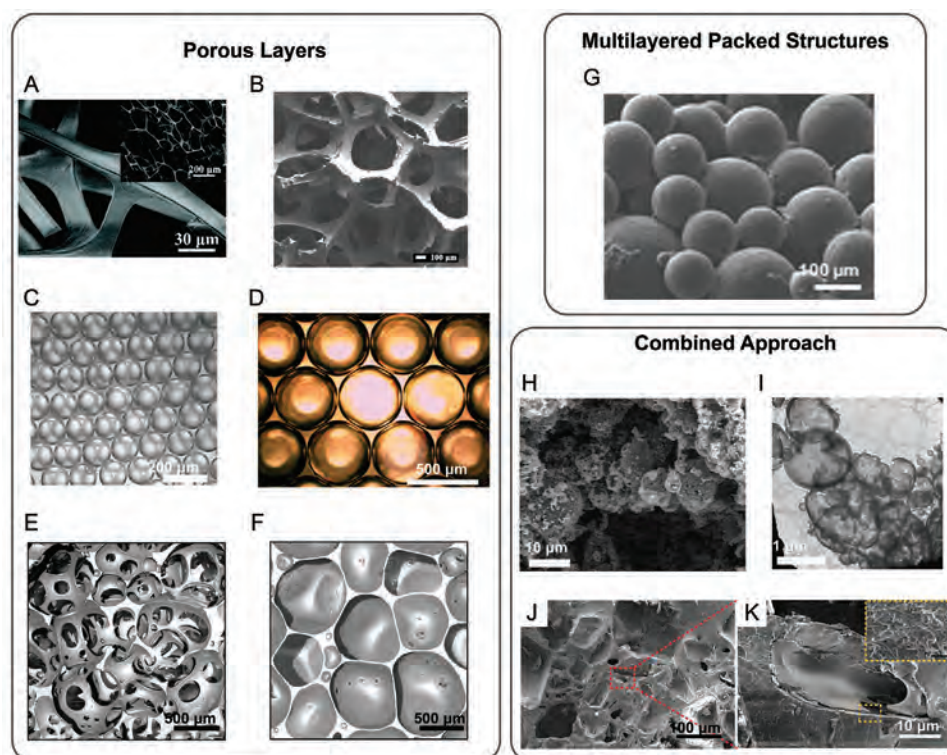


**Figure 11.** Microscope images of fabricated porous layers, multilayered packed structures, and combined approach structures. A) SEM image of the template sponge. Adapted with permission.<sup>[117]</sup> Copyright 2018, The Royal Society of Chemistry. B) SEM image of the coated polyurethane foam. Adapted with permission.<sup>[118]</sup> Copyright 2018, American Chemical Society. C) Optical microscope image of closely packed 100  $\mu\text{m}$  droplets. Adapted with permission.<sup>[87]</sup> Copyright 2018, American Chemical Society. D) Optical microscope image of closely packed 500  $\mu\text{m}$  droplets. Adapted with permission.<sup>[87]</sup> Copyright 2018, American Chemical Society. E) Micro-CT scan of open-cell polymer foams. Adapted with permission.<sup>[112]</sup> Copyright 2019, Wiley-VCH. F) Micro-CT scan of closed-cell polymer foams. Adapted with permission.<sup>[112]</sup> Copyright 2019, Wiley-VCH. G) SEM image of nanotube-wrapped PDMS microspheres. Adapted with permission.<sup>[106]</sup> Copyright 2018, Elsevier B.V. H) SEM image of the hollow sphere structures. Adapted with permission.<sup>[104]</sup> Copyright 2014, Macmillan Publishers Ltd. I) Transmission electron microscopy (TEM) of the hollow sphere structures. Adapted with permission.<sup>[104]</sup> Copyright 2014, Macmillan Publishers Ltd. J, K) Cross-sectional view SEM image of HPM-PDMS film. Adapted with permission.<sup>[63]</sup> Copyright 2019, American Chemical Society.

exposed surface. This micropatterned PDMS could then be used to mold an elastomer/conductor mixture to yield a patterned active layer (Figure 12B). A similar structure can also be achieved by prestraining a material coated with a conductive precursor like graphene oxide (Figure 12C).<sup>[119]</sup> Jia et al. applied a strain to 3M very high bond (VHB) tape and then coated it in an aqueous graphene oxide solution that forms stable bonds with the VHB tape after drying.<sup>[119]</sup> Hydrazine hydrate was then used to partially reduce the graphene oxide interlayer into conductive graphene. Since this reduction reaction produces a gaseous product, a partially reduced graphene oxide interlayer expansion structure was formed in the process. This caused the formation of a dome-like microstructure expansion of the underlying reduced graphene oxide layer while also producing the necessary conductive layer. Once the VHB tape was released, skin-like wrinkles with microdomes were realized (Figure 10K–M).<sup>[119]</sup>

### 3.3.2. Porous Layers

Porous materials have been used frequently to improve the sensitivity of resistive pressure sensors (Figure 11A–F).<sup>[56,87,114,117,118,122–124]</sup>

The reason for this is that the sensitivity of resistive pressure sensors based on rubber materials is dependent on the deformability of the material and, in general, a porous material is more deformable than its equivalent bulk material.<sup>[56,125]</sup> Moreover, as compared with mold casting techniques, porous layers allows for more 3D microengineering of the active layer, which improves the nodes where contact area can be increased, thus potentially improving the sensitivity.<sup>[87]</sup>

One simple way of fabricating porous active materials for resistive sensors is to take an already porous material, such as a melamine or polyurethane sponge, and coat it with a conductive layer (Figure 11A,B).<sup>[117,118,123]</sup> This process can be done by dipping or immersing the sponge into the desired conductive solution (Figure 13A). Since the conductive sponge is more 3D than a micropatterned material, there are more potential connections that can be made, potentially leading to a higher resistance change for a given applied pressure as compared to single-layer micropatterns. A major advantage of this technique is the ability to use commercially available materials as the conductive layers, with little to no processing needed. Since the materials are commercially available, large-area fabrication is easier and more economical.<sup>[117,118]</sup>

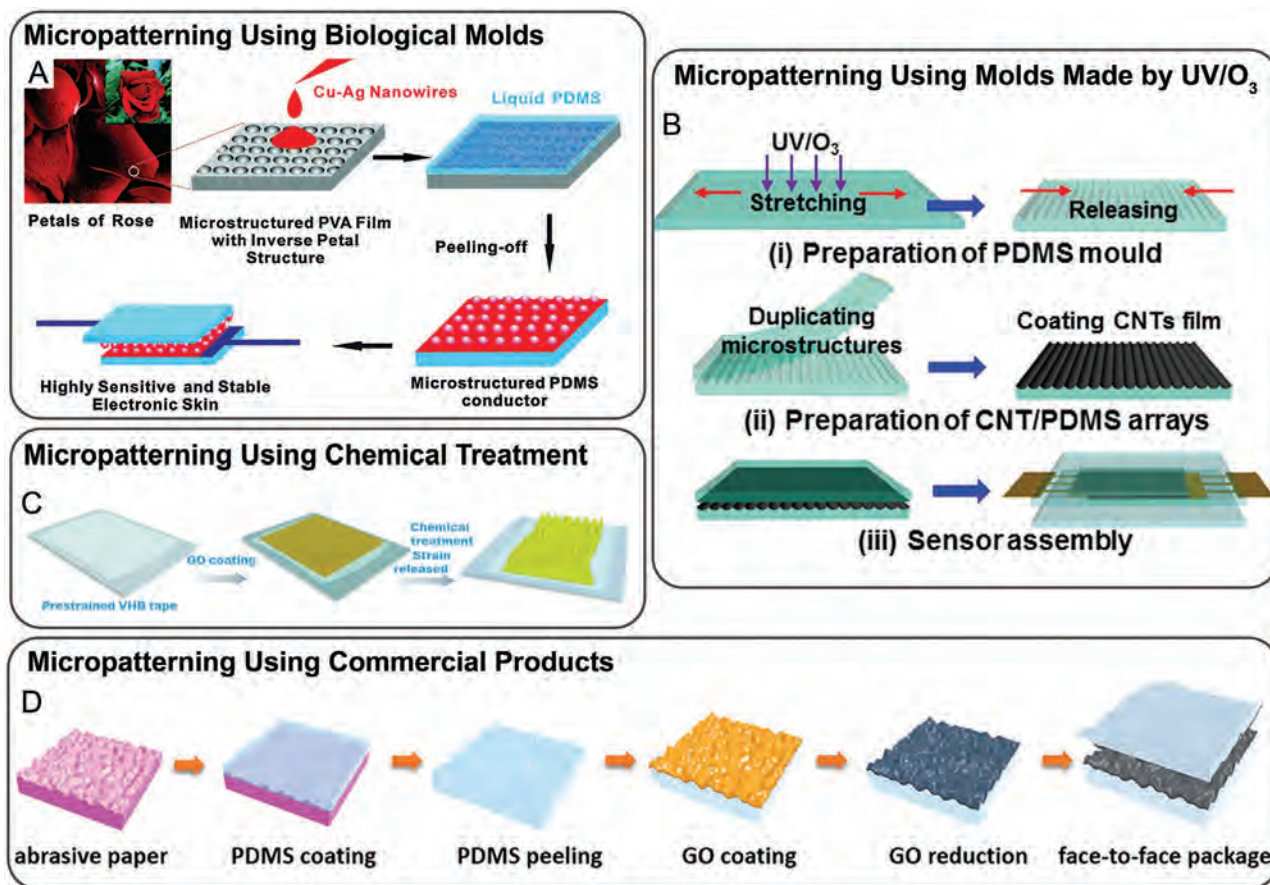


**Figure 12.** Schematics of fabrication methods to make micropatterned structured. A) Schematic of the fabrication process using a rose petal to mold the elastomer layer (Figure 10H). Adapted with permission.<sup>[110]</sup> Copyright 2015, The Royal Society of Chemistry. B) Schematic of fabrication process using molds made by UV/O<sub>3</sub> (Figure 10J). Reproduced with permission.<sup>[23]</sup> Copyright 2018, IOP Publishing Ltd. C) Schematic of fabrication process to make skin-like wrinkles or lines using VHB tape that was coated and then chemically treated to produce the final structure (Figure 10K–M). Adapted with permission.<sup>[119]</sup> Copyright 2019, The Royal Society of Chemistry. D) Schematic of the fabrication process using abrasive paper to mold the elastomer layer, followed by coating and packaging to make the resistive pressure sensor. Adapted with permission.<sup>[103]</sup> Copyright 2018, American Chemical Society.

One of the major challenges of using a commercially available material as the template for the active layer is the lack of control of pore size and structure, which can impact reproducibility and tunability of the sensor structure and performance. One way to address this challenge is to either fabricate a 3D template structure and subsequently etch away the template<sup>[126]</sup> or to cure the active material around a material that can be subsequently etched away.<sup>[127,128]</sup> Kim et al. developed a new process to create porous structures for resistive pressure sensors (Figure 11C,D).<sup>[87]</sup> As previously discussed, they developed DMESA, which involves surfactant-stabilized aqueous droplets in the oil solution to fabricate porous active layers with uniformly sized spherical micropores, providing a more controllable technique for creating porous active layers (Figures 4I and 6A).<sup>[87]</sup> This technique is economical, has improved spatial uniformity, removes the need for a template, and improved tunability of the microstructure size. The droplet size can be easily tuned by adjusting the aqueous to oil flow rate (Figure 13B). To make this technique advantageous for resistive pressure sensors instead of capacitive pressure sensors, the structure can be functionalized with multiwalled carbon nanotubes to make it the active layer of the sensor.<sup>[87]</sup>

Similar to DMESA, direct bubble writing has also been used to achieve a porous conductive structure with controllable pore sizes (Figure 11E,F).<sup>[112]</sup> The structure can be tuned to be either an open- or closed-cell foam by printing air-filled or nitrogen-filled bubbles, respectively (Figure 13C,D). This high throughput process uses a printhead that controllably ejects liquid shell gas-core droplets through a core-shell nozzle onto a designated substrate where they are quickly photopolymerized (Figure 13E).<sup>[112]</sup> By manipulating the gas pressure and the ink flow rate, the final porous structure can be changed. The ink can be controlled from a constant flow of pure liquid to mono- and bidispersed bubbles to burst bubbles with no directionality (Figure 13F,G).<sup>[112]</sup> Silver nitrate predissolved into the liquid ink can subsequently be reduced with UV light into silver nanoparticles to render the resulting porous material conductive. As such, this new method provides a highly controllable and high throughput option to fabricate a porous conductive structure for larger pore sizes down to several hundreds of microns in diameter.<sup>[112]</sup>

Micropores have been introduced to the active layer materials of resistive pressure sensors in order to improve the sensor performance, especially sensitivity. Some of the techniques may not be as tunable and predictable as micropatterns due to the



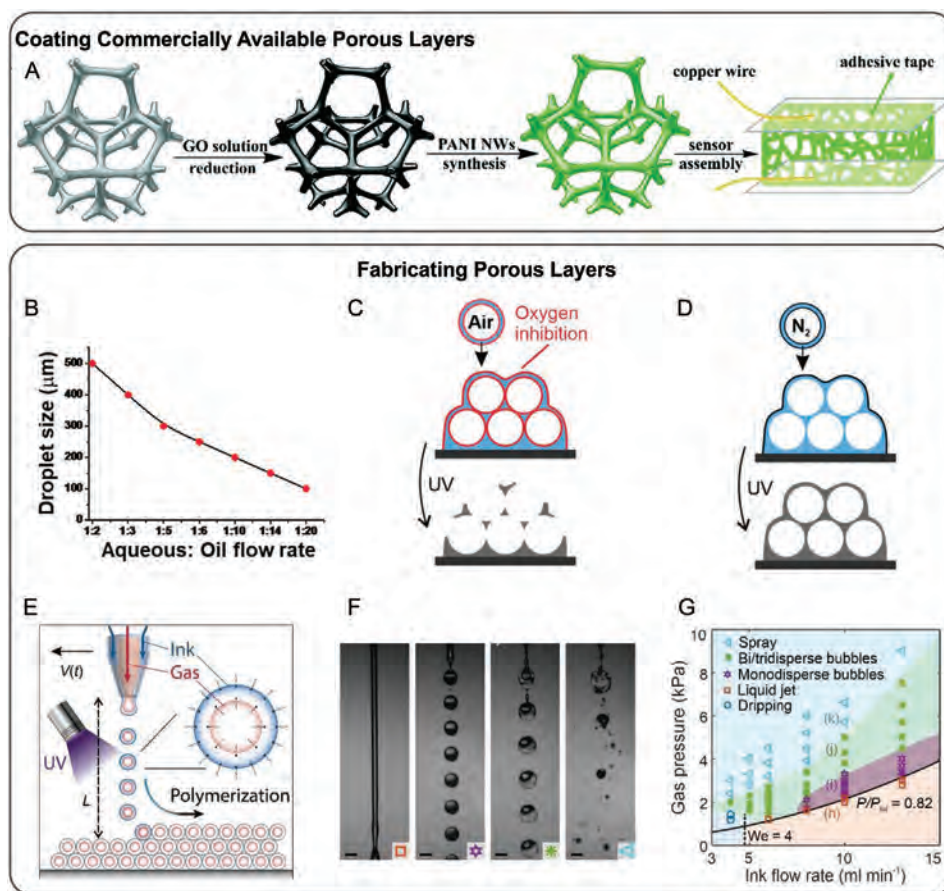


**Figure 13.** Fabrication processes of porous layers and their tunability. A) Porous active layers can be made by directly coating commercially available sponges (Figure 11A), as shown in the schematic. Reproduced with permission.<sup>[117]</sup> Copyright 2018, The Royal Society of Chemistry. B) The droplet size (Figure 11C,D), and consequently the pore size, can be tuned using the aqueous to oil flow rate in the DMESA process. Reproduced with permission.<sup>[87]</sup> Copyright 2018, American Chemical Society. C) Open-cell porous layers structures (Figure 11E) can be formed using printing of air-filled bubbles. Adapted with permission.<sup>[112]</sup> Copyright 2019, Wiley-VCH. D) Closed-cell porous layer structures (Figure 11F) can be formed using printing of nitrogen-filled bubbles. Adapted with permission.<sup>[112]</sup> Copyright 2019, Wiley-VCH. E) Schematic of fluid shell, gas core bubbles ejected from a core-shell printing nozzle onto a surface where it is rapidly polymerized. This is the basis for a process to make porous layers called direct bubble writing. Adapted with permission.<sup>[112]</sup> Copyright 2019, Wiley-VCH. F) In direct bubble writing, low gas pressure results in a continuous stream (orange square), intermediate gas pressures results in monodisperse (purple star) or bidisperse (green asterisk) bubbles, and high gas pressures may produce burst bubbles (blue triangle). Adapted with permission.<sup>[112]</sup> Copyright 2019, Wiley-VCH. G) In direct bubble writing, a phase diagram of gas pressure as a function of ink flow rate demonstrates the tunability of the final structure by varying those two parameters. Reproduced with permission.<sup>[112]</sup> Copyright 2019, Wiley-VCH.

variability in pore size and limited control over their uniformity. However, since the sensitivity of resistive sensors is dependent on increased contact area in the active layer, the 3D structure may be advantageous over micropatterned counterparts.

### 3.3.3. Multilayered Packed Structures

Another method of creating resistive pressure sensors is by creating multilayered packed structures, one method of which is coating prefabricated elastomer microspheres with a conductive layer (Figure 11G).<sup>[106]</sup> Similar to other techniques, air voids between the structures increase the deformation of the active layer upon loading of external pressures, which increases the change in contact area for a given pressure, consequently enhancing sensitivity. Elastomeric microspheres can be easily prepared using emulsion polymerization, a process that is both

scalable and environmentally friendly.<sup>[106,129]</sup> Xu et al. used this technique to make a resistive pressure sensors comprising conductive microspheres between 20 to 100  $\mu\text{m}$  in diameter. To make the microspheres, PDMS base and curing agent were emulsified within polyvinyl alcohol prior to curing. Once cured, the emulsion was centrifuged and washed to remove polyvinyl alcohol from the microsphere surface. The microspheres were then coated with carbon nanotubes to make them conductive.<sup>[106]</sup>

Alternatively, preexisting micropatterning techniques have been used to fabricate micropatterned structures that are then stacked to create multilayered packed structures.<sup>[110]</sup> A unique method to prepare the molds for these patterns is using a static breath figure method.<sup>[115,130]</sup> Wang et al. prepared porous polystyrene template using this method, whereby they evaporated a volatile solvent from a polystyrene surface in a humid environment. The rapid evaporation caused a temperature drop on the substrate surface, causing water droplet nucleation and growth.



#### Fabrication Using a Combined Approach

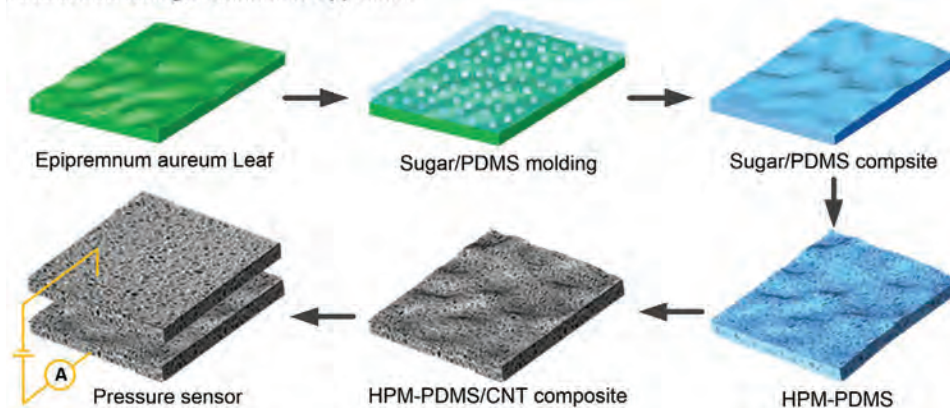


**Figure 14.** Fabrication process using a combined approach. The micropatterned structure was made using *E. aureum* leaves as molds. The pores were made using sugar microparticles that were dissolved after curing to achieve the final structure (Figure 11J,K). Reproduced with permission.<sup>[63]</sup> Copyright 2019, American Chemical Society.

The water droplets self-assemble into hexagonally close-packed 3D arrays, and upon complete evaporation of the solvent and water droplets, an inverse dome structure remains on the polystyrene surface. This mold could then be used to make the multilayered dome structure.<sup>[115]</sup>

As with porous structures, multilayered packed structures allow for a more 3D active layer structure because the spheres can be easily stacked. One major advantage of this method is that it can be fabricated completely in the laboratory and is not dependent on highly specialized materials or equipment. Further, the 3D structure increases the number of potential contact points that can be generated or increased in area with the applied pressure. However, as compared to using readily available materials, this process may be more time intensive. As compared with highly controllable processes such as photolithography-based molding, there is likely to be greater variance between sensors and lower predictability.

#### 3.3.4. Combined Approaches

There has been increased interest in combining multiple approaches to microengineering the active layer of resistive pressure sensors in order to leverage their different performance advantages. For example, Pan et al. designed hollow-sphere conductive hydrogel microstructures (Figure 10H,I) and then micropatterned the film using a molding technique.<sup>[104]</sup> By incorporating hollow sphere structures, they enabled the conducting polymer polypyrrole, a generally stiff and brittle material, to elastically deform when pressure is applied and released, while still maintaining its capabilities to withstand high stresses and strains. Once the hydrogel micropattern layer was made, it was further molded using a wafer mold with the shape of lines with a triangular cross-section profile prior to gelling. Although the hollow spheres already helped improve the sensitivity of the sensor compared to a bulk material, additional patterning of the layer markedly increased the sensitivity further.<sup>[104]</sup>

Another combined approach with the same goal is a hybrid porous microstructure/micropattern done by Zhao et al. (Figure 11J,K).<sup>[63]</sup> The micropatterned structures were molded

using *Epipremnum aureum* leaves, while the pores were made by mixing in soluble sugar particles that were later removed (Figure 14). The resulting material was rendered conductive by coating with multiwalled carbon nanotubes. Finally, a multilayered structure was achieved by stacking two of these hybrid porous microstructured/micropatterned films together. Although time-intensive, this designed device was found to have much stronger performance than its only porous or only microstructured/micropatterned counterpart, as previously discussed.<sup>[63]</sup> Thus, although it adds a level of complexity to the fabrication process, a combined approach may be advantageous for particular applications that demand even higher sensitivities and lower detection limits, such as for electronic skin.

### 3.4. Comparison of Fabrication Methods and Techniques

There are several considerations when choosing a method of microengineering the active layer of a sensor, including ease of fabrication, active layer uniformity, shape and size versatility and tunability, and uniformity, and scalability. The importance of each of these considerations can vary depending on the specific application, equipment availability, and material accessibility. Many of the fabrication considerations are similar to their capacitive pressure sensor counterparts. Photolithographic methods produce highly uniform and tunable structures but the mold fabrication is more complex and more costly. However, using a commercially available material may be more scalable and simpler, but the tunability and uniformity of the structure may be compromised.

#### 3.4.1. Ease of Fabrication

Ease of fabrication is an important consideration, particularly as sensor development progresses toward commercialization. Because mold fabrication is not required, techniques that use biological or commercially available materials as the mold or template for the active layer can be considered advantageous in this regard.<sup>[103,105,109,110,117]</sup> Nevertheless, once a mold is

produced, for instance using photolithographic methods, it can typically be reused repeatedly.

Although adding the need to fabricate a mold adds another level of complexity to the fabrication process, the level of complexity varies between methods. For example, unlike photolithography, 3D printing is a fabrication process that simplifies the mold fabrication process and limits the time and labor necessary to mold the active layer.<sup>[97]</sup> 3D printing is not a labor-intensive process, and thus this fabrication process is considered easier than photolithography, but more challenging than having the mold or template readily available. Another technique that has been used that would be similarly classified is making the foam or sponge-like template for the active layer as opposed to using a commercially available material because it is a relatively easy process but requires fabrication of the template.<sup>[118]</sup>

Finally, one distinctive feature of resistive sensors is the incorporation of conductive materials in the active layer, which may add a layer of complexity to the fabrication process. There are two main approaches: coating the surface of the structured component (e.g., by drop casting, spray coating, or immersing in a conductive solution) or directly mixing a conductive material or precursor into the structure. While coating can be a straightforward, drop-in method to render microstructures conductive, maintaining good adhesion between the coating and the underlying elastomer can be a challenge. Adhesion, and therefore durability, can be improved via chemical bonding interactions between the coating and elastomer; for instance, Yang et al. coated their PDMS structures with polypyrrole because the conducting polymer can bond with the hydroxyl groups on the PDMS surfaces.<sup>[75]</sup> Meanwhile, directly incorporating conductive materials into the microengineered elastomer simplifies the fabrication process, though it provides poorer control over morphology, which can impact the resistance response to pressure. Thus, when considering the application of a sensor, the ease of the fabrication process of the entire sensor must be taken into account to ensure the process does not become a restrictive limitation.

### 3.4.2. Active Layer Uniformity

Uniformity of the active layer refers to the shape and size consistency of the micropattern, sphere, and voids within a sensor and between sensors of the same type and can affect several parameters of the sensor. Structural uniformity is critical to achieve performance uniformity, a particularly important factor in pressure sensor arrays.<sup>[124]</sup> High uniformity of the active layer is often achieved using precise fabrication of the mold, such as 3D printing, enabling a highly uniform active layer.<sup>[97]</sup>

Some fabrication methods provide partial but not full control over the uniformity of the micro-engineered active layer. For example, directly lasereng the elastomeric material allows for similar shapes and spacing, but the uniformity is lower than that of a process like photolithography or 3D printing that is highly precise (Figure 8B). It is important to note that although the 3D printing resulted in a highly uniform mold, the feature size was significantly larger than those attempted with the direct lasereng process. This distinction is important as scaling down the feature size may be challenging for the 3D printing process. The photolithography process, though, can achieve as

highly uniform  $\approx 20\text{ }\mu\text{m}$  features as the direct laser process, and can even achieve this with smaller features. However, some techniques may be able to achieve uniformity in one part of the fabrication process, but not in another. An example of this is the combined approach utilized by Pan et al., for which the micropatterning done using the fabricated mold achieves high uniformity, but the hydrogel microspheres lead to more variability (Figure 11G). This results in an active layer with a uniform micropattern but nonuniform hollow spheres. Finally, as previously discussed, low uniformity of the micro-engineered active layer is common when using commercial or biological materials.

### 3.4.3. Shape and Size Versatility and Tunability

The versatility and tunability of the size and shape of the microstructures can be very valuable when trying to tune the sensitivity of a sensor. The more control there is over the shape and size of the microengineered active layer, the greater the control over the sensor performance. A low level of versatility and tunability can be used to classify fabrication methods that cannot tune size or shape. For example, when using commercial or biological materials as a mold or template for the active layer microengineering, the user has no control over the shape and size of structures—it is predetermined either biologically or industrially.<sup>[101,105,109,110,117]</sup> The same is true for the fabrication process of plasma treatment of PDMS upon stretching and then releasing the stretch. Although there is little control over the size of the structure, the amount of stretching may provide minimal control over the structure size.<sup>[23,76]</sup>

However, there are techniques used to make resistive pressure sensors with microengineered active layers that provide more versatility and tunability of either the shape or size of the structures. For example, using the DMESA and direct bubble writing methods allows for tunability of the size of the micropores by adjusting flow rates, but the shape is not tunable as it can only be used to make microsphere shapes.<sup>[87,112]</sup> Alternatively, a method such as directly lasereng the elastomer for the active layer is tunable in its shape and size, but the tunability is limited by the capabilities of the laser itself.<sup>[107]</sup> Usage of photolithographic techniques seems to be the more versatile and tunable method within the discussed size range. Understanding the tunability and versatility of the technique being used to create the microstructures is vital to the performance of the resistive sensor. If using a technique that is highly tunable, changing the sensor performance is more easily achievable using the same fabrication method. As a result, it is important to consider the tunability and versatility of the technique chosen for the specific application based on the restrictions of the application.

### 3.4.4. Scalability

When looking toward industrial applications, it is important to consider the ease of scalability of both the fabrication process and the sensor itself.<sup>[39]</sup> The latter is important when considering making the sensor larger or making an array, such as for electronic skin applications which may require covering a large

area. These are both important parameters because they make the sensor industrially relevant.<sup>[39]</sup> A technique that requires intimate, hands-on fabrication or a process that is costly may not be scalable. To address this issue, several works specifically discuss the scalability of their processes. For example, using biomaterials or commercially available materials allows for easily made or purchased molds, making the scaling process economical and simpler.<sup>[105,109,110,117]</sup>

Alternatively, using a simple and scalable technique to make a template for the active layer of a resistive pressure sensor can be advantageous industrially, as well. This is true for the process of elastomer microspheres assembly to fabricate the active layer, especially when the elastomer is commercially available, such as PDMS, since this process is both simple and scalable.<sup>[106]</sup> Similarly, by removing the need to fabricate each mold and using a high throughput method to fabricate the active layer, a scalable process emerges, as is the case with direct bubble writing.<sup>[112]</sup> Thus, it is important when approaching a sensor application to consider whether the sensor and fabrication process can be scaled-up to envision the potential of product commercialization.

## 4. Piezoelectric Pressure Sensors

Piezoelectricity describes the ability of certain materials to generate a voltage in response to an applied pressure. The applied pressure results in a change in the separation between dipoles in the material, which leads to a buildup of charges on the electrodes.<sup>[131,132]</sup> Examples of piezoelectric materials include polyvinylidene fluoride (PVDF), lead zirconate titanate (PZT), and zinc oxide (ZnO).

In piezoelectric nanogenerator-based sensors, mechanical inputs are converted to electrical outputs without applying external power sources. These are considered self-powered active sensors.<sup>[133]</sup> In order to understand the properties of piezoelectric sensors, Hooke's Law is combined with an equation for electrical behavior.<sup>[134]</sup> Hooke's Law is defined as

$$S = sT \quad (4)$$

Where  $S$  is the strain,  $s$  is the compliance, and  $T$  is the applied stress.<sup>[111]</sup> The equation for electrical behavior is

$$D = \epsilon E \quad (5)$$

Where  $D$  is the electric charge density displacement,  $\epsilon$  is permittivity, and  $E$  is electric field strength. These equations can then be linearly approximated to

$$S = s^E T + dE \quad (6)$$

$$D = dT + \epsilon^T E \quad (7)$$

This confirms that changes in strain will result in a change in piezoelectric output.<sup>[135,136]</sup> As a result, there has been significant interest in piezoelectric sensors due to their extended lifetime, scalability, and lack of need for recharging.<sup>[137]</sup>

Piezoelectric sensors generally do not require an external power source for the sensor layer to operate, but are more suitable for dynamic sensing and will experience temperature sensitivity and higher drift in response over time.<sup>[14,28,36,38,49,57]</sup> As with other types of pressure sensors, the performance

of piezoelectric pressure sensors can be greatly improved by microengineering the active layer (**Figure 15**).<sup>[38,134,138,139]</sup> Although there is limited work done using microengineered active layers for piezoelectric pressure, there is evidence that this method can be integral in improving sensor performance.<sup>[38,134,138]</sup> In the following section, we will briefly review the few examples that have been reported of microengineering strategies for piezoelectric sensors, simultaneously discussing design considerations and their corresponding fabrication methods.

### 4.1. A Brief Introduction to Geometric Microengineering of Piezoelectric Sensors

Reported microengineering techniques for piezoelectric sensors have largely entailed using micropatterning to structure the piezoelectric active layer. Despite the limited examples of microengineering so far, future work may apply the many capacitive sensor microengineering approaches (Section 2.1) toward structuring piezoelectric materials. Because piezoelectric pressure sensors are based on the strain response for a given stress, the microengineered active layer designs that showed the strongest performance for capacitive pressure sensors should also be advantageous piezoelectric pressure sensors, unlike resistive pressure sensors whose performances are generally dependent on changes in contact area.

Micropatterning of the piezoelectric active material has proven to be an effective method for enhancing the performance of piezoelectric pressure sensors. For instance, micropatterned P(VDF-TrFE) was shown to improve the power output of the nanogenerator by nearly five times compared to that of a flat film-based piezoelectric nanogenerator when a 0.15 kgf force was applied.<sup>[134]</sup> Improved voltage and current are attributed to the different strain that results from the different shape types and the air voids as compared with a flat film (**Figure 15A**). Clearly, simply introducing a microengineered active layer plays an integral role in improving the piezoelectric response, and can help produce even higher performing piezoelectric pressure sensors in the future.

Similar to the previously discussed types of pressure sensors, the performance can be further tuned by changing the compressibility of the active layer, something that is done by carefully choosing the feature shape, dimensions, and interfeature spacing.<sup>[134]</sup> Similar to capacitive pressure sensors, Lee et al. found that the pyramid-shaped micropatterned sensor was more stable with better performance compared to the trigonal line-shaped micropattern or just the traditional flat P(VDF-TrFE) piezoelectric nanogenerator (**Figure 15B–D**).<sup>[134]</sup> The trigonal line-shaped micropattern is similar to the microcylinder line shapes, but the cross-section is a triangle as opposed to a dome or a cylinder. Using finite element modeling, Lee et al. showed more than a fivefold increase in the strain of the trigonal microstructure shape in response to an applied stress as compared to a flat thin film, improving the voltage by more than four times, allowing the pressure sensor to be self-powered.<sup>[134]</sup> This was even more significant when comparing the pyramid micropattern to the flat thin film, the former of which produced more than 60 times the strain and almost fifty times the voltage



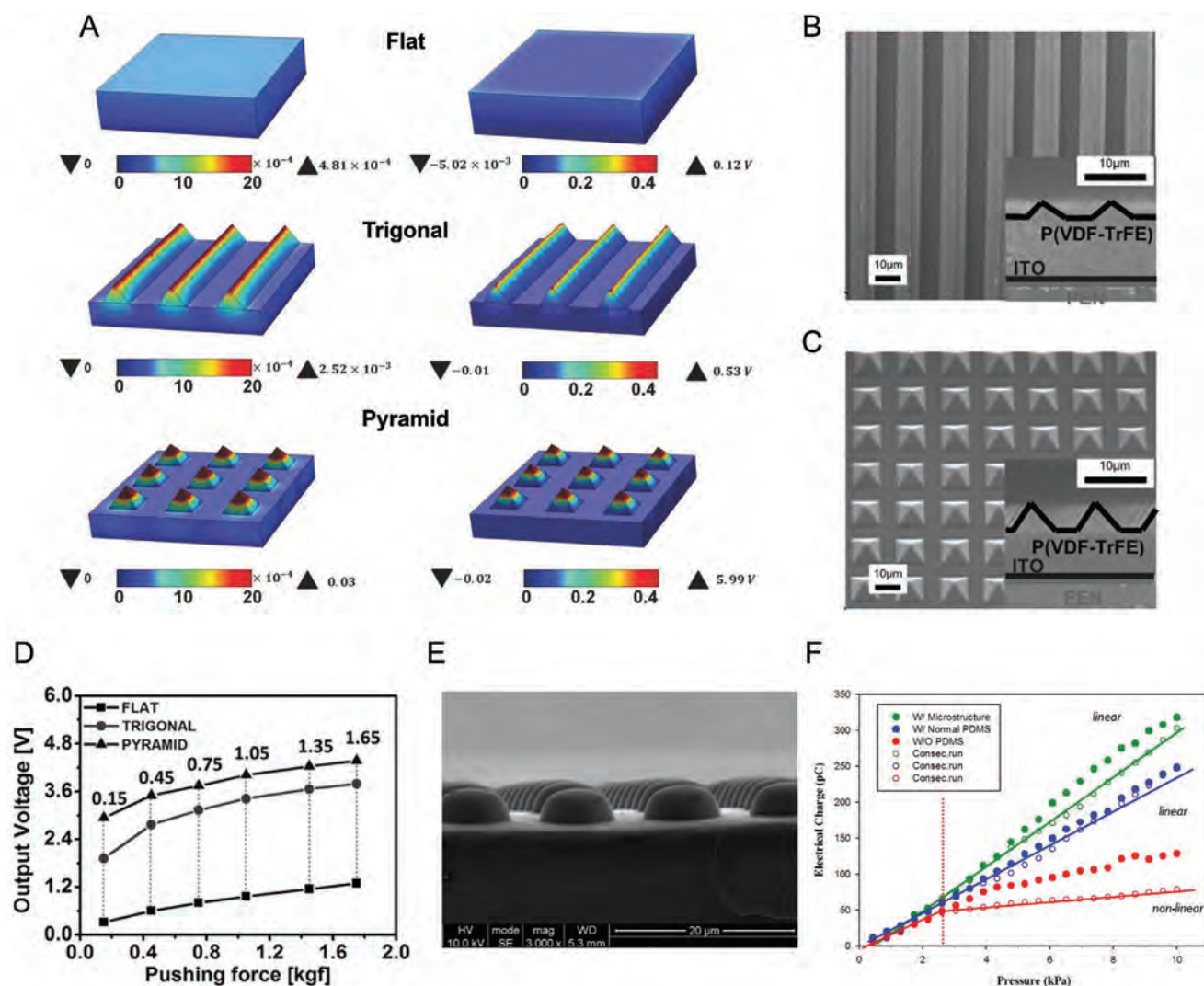


**Figure 15.** Tunability of micropatterned structures and hollow structures for piezoelectric pressure sensors. A) Simulation results of devices with micropatterned structures—flat panel (top), trigonal or line (middle), and pyramid (bottom)—and their response to 0.1 kgf applied force. Right panel is strain response to applied stress. Left panel is voltage response to applied stress. Adapted with permission.<sup>[134]</sup> Copyright 2015, Wiley-VCH. B) FESEM images of trigonal micropatterned P(VDF-TrFE) fabricated from a mold made by photolithography. Inset is the cross-sectional image of the structure. Reproduced with permission.<sup>[134]</sup> Copyright 2015, Wiley-VCH. C) FESEM images of pyramid micropatterned P(VDF-TrFE) fabricated from a mold made by photolithography. Inset is the cross-sectional image of the structure. Reproduced with permission.<sup>[134]</sup> Copyright 2015, Wiley-VCH. D) Comparison of the output voltages for unstructured, trigonal micropatterned, and pyramid micropatterned piezoelectric pressure sensors for a range of external forces. Reproduced with permission.<sup>[134]</sup> Copyright 2015, Wiley-VCH. E) An SEM image of the circular dome microstructures fabricated from a mold made by photolithography. Adapted with permission.<sup>[38]</sup> Copyright 2014, AIP Publishing LLC. F) Micropatterned PDMS shows a stronger electrical response to applied pressure as compared to the same device without PDMS or with unstructured PDMS. Reproduced with permission.<sup>[38]</sup> Copyright 2014, AIP Publishing LLC.

output for the same applied pressure and starting device thickness.<sup>[134]</sup> Understanding the difference in compressibility of the different microengineered layers is integral because higher strain results in higher piezoelectric signal, and consequently, higher output voltage and current.<sup>[134]</sup>

From a fabrication standpoint, micropatterned piezoelectric materials can be realized using the same methodologies as have been used to micropattern the dielectric materials in capacitive pressure sensors. Specifically, one of the most common methods of achieving this is using a silicon mold made with photolithography.<sup>[38,134]</sup> For instance, piezoelectric pyramid

structures can be fabricated by first fabricating a mold, by using potassium hydroxide to nonuniformly etch a silicon wafer into pyramidal or trigonal line structures (Figure 15B,C).<sup>[15,134]</sup> Circular trenches, as opposed to pyramid structures, can also be fabricated using photolithography and deep reactive ion etching (Figure 15E).<sup>[38]</sup> Dome micropatterns of piezoelectric material can then be directly molded using a replica technique once the mold itself is surface-functionalized with a material to prevent adhesion, for instance by using a trichloro(1H, 1H, 2H, 2H-perfluorooctyl)silane surface treatment on PDMS.<sup>[17,38,71]</sup> Although few methods of micropatterning have been used to

improve piezoelectric pressure sensor performance, many of the previously discussed techniques used for resistive or capacitive pressure sensors can be utilized for these sensor types, as well.

## 5. Triboelectric Pressure Sensors

Triboelectric nanogenerators have been of particular interest recently as a promising energy conversion mechanism for personal electronics.<sup>[61,140,141]</sup> They were first reported in 2012 by Fan et al. with their principle being the conversion of mechanical energy into electrical power.<sup>[62,142]</sup> Triboelectric generators provide an alternative method to piezoelectric nanogenerators by using different physical mechanisms for generating electricity.<sup>[142]</sup> Triboelectric nanogenerators are based on the coupling effect of contact electrification and electrostatic induction.<sup>[143–145]</sup> The working principle of triboelectric active sensors is similar to triboelectric nanogenerators.<sup>[61]</sup> They can monitor both static and dynamic pressure sensing by changing the measurement tactics, which can be important depending on the desired application.<sup>[61]</sup> For static pressure detection, open-circuit voltage with transferred charge density is employed. For dynamic pressure detection, pulse-like short-circuit current peaks are employed.<sup>[61]</sup>

Triboelectric nanogenerators are considered a promising field for pressure sensors due to their low cost, high power density, and simple design. Most importantly, similar to piezoelectric pressure sensors, triboelectric pressure sensors can also be self-powered.<sup>[145–147]</sup> While microengineering has thus far been largely unexplored for triboelectric pressure sensors, recent work demonstrates its potential to significantly enhance sensor performance.

### 5.1. Geometric Microengineering of Triboelectric Pressure Sensors

Microengineering the active layer of triboelectric pressure sensors is of particular interest because charges are generated through contact electrification, making the surface structure integral to improve sensor performance.

Two recent works have highlighted the use of microengineering for triboelectric pressure sensors.<sup>[61,62]</sup> Each uses a different method of micropatterning that has been previously discussed: photolithography<sup>[61]</sup> and molding using commercially available materials.<sup>[62]</sup> Lin et al. developed a triboelectric pressure sensor that can detect both static and dynamic pressures using pyramid microstructures placed on a gold electrode substrate.<sup>[61]</sup> The microstructures interact with a composite of silver nanowires and nanoparticles to induce the triboelectric effect upon compression. The micro and nanostructures were used in order to increase contact area between the two surfaces to enhance the triboelectric effect, similar to the advantages of microengineering the active layer in resistive pressure sensors.<sup>[61]</sup> By utilizing these structures, Lin et al. achieved a sensitivity of  $0.31 \text{ kPa}^{-1}$ , response time of less than 5 ms, and a detection limit of 2.1 Pa with a stable performance over 30 000 tested cycles.<sup>[61]</sup> These results are comparable to some of the

best sensors of other pressure sensor types with the advantage of being self-powered.

Alternatively, Das et al. developed a low cost, eco-friendly triboelectric pressure sensors using micropatterned PDMS molded with commercially available sandpaper to achieve even higher sensitivity.<sup>[62]</sup> PDMS solution was spincoated on the sandpaper, allowed to cure, and finally demolded with the micropattern.<sup>[62]</sup> With these micropatterned triboelectric pressure sensors, the charging occurs due to iterative physical contact between the micropatterned PDMS and a flat surface with a different polarity. Using this sandpaper as a mold, Das et al. were able to fabricate a sensor with a sensitivity of  $7.697 \text{ kPa}^{-1}$ , response time of less than 9.9 ms, and a detection limit of approximately 1 Pa.<sup>[62]</sup> It is important to note that the best response time may be due to frequency of signal detection of the available equipment as opposed to the sensor itself. Similar to the triboelectric pressure sensor designed by Lin et al., this is comparable to the best pressure sensors of different sensor types. As a result, triboelectric pressure sensors with microengineered active layers are a promising option for self-powered, high performing pressure sensors that can greatly benefit from microengineering of the active layer.

## 6. Conclusions and Outlook

Pressure sensors—sensors that respond to normal applied force—play an integral role in many industries, including the healthcare sector and robotics, where there is an increasing demand for more specialized and higher-performing pressure sensors. Micro-engineering the active layer of the sensors is the key to addressing this demand. In this review, we highlighted different methods of micro-engineering the active layers of a wide range of pressure sensors and the efforts made towards creating higher performing pressure sensors. Methods include micropatterned structures, porous layers, multilayered packed structures, and combined approaches, all of which provide a unique capability of improving pressure sensor performance without needing to design new materials. Each of these types of microengineered layers has different effects on the performance of the pressure sensor, including sensitivity, maximum sensitivity range, limit of detection, response time, and relaxation time. Additionally, the experimental fabrication methods used to achieve these different microengineered structures also have unique advantages and disadvantages to consider, including reproducibility and scalability, particularly as sensors scale toward commercialization. While several strategies of achieving scalable sensors for industrial applications have been discussed in this work, there still remains uncertainty as to the how important each of the factors is in scalability. This can be addressed in the future through industrial scale-up efforts.

By using microengineering, capacitive, resistive, piezoelectric, and triboelectric pressure sensors with very high sensitivities and very low detection limits have been achieved, with some even achieving high working ranges as well. These high-performing sensors have been able to address some of the emerging requirements of pressure sensors and have been used in exciting demonstrations of their potential, including tactile sensing, noncontact heartbeat and respiration, and health

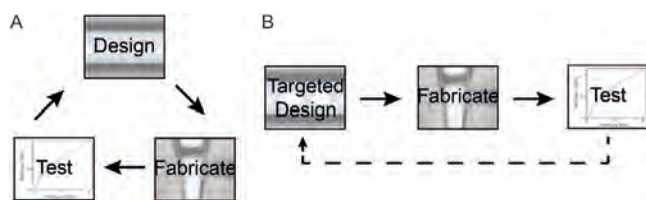


**Figure 16.** Models of fabricating sensors for specific applications. A) Current methods require a more circular approach to designing pressure sensors. B) By being able to better predict pressure sensor performance, we are able to more targetedly design sensors for specific applications, making it a more linear design and fabrication process. Reproduced with permission.<sup>[71]</sup> Copyright 2019, Wiley-VCH.

monitoring. Many of these applications require the encapsulation of the sensors, which has the potential to diminish the sensitivity by partially compressing the microengineered layer. As a result, further work must be done to address packaging of the sensors with minimal effect on the microengineered layer.

Despite the rapid progress and wide range of approaches to microengineering the active layers of pressure sensors, further work still needs to be done to better quantitatively compare between sensors of different types, which can be challenging given the variety of sensing mechanisms. Additionally, there is still a lack of clarity as to the best microengineering method for each pressure sensor type, in part due to the impact of the materials used for the active layers on the performance. While comparisons have been made between, for instance, the efficacy of different micropatterned shapes, there has not yet been a rigorous comparison between the performance achievable by different micro-engineering design strategies, such as a comparison between micropatterned and porous structures.

Computational modeling efforts will help to bridge this gap in knowledge and enable more rigorous comparisons that will pave the way for new and improved microengineering strategies to be developed. It is integral to be able to understand the effects of each of the microengineered designs on a wide range of performance parameters—not only the strain experienced for a given applied stress—since different applications demand different sensor characteristics. Coupled with experimental validation and fabrication innovations to improve reproducibility and uniformity, these modeling efforts will pave the way for the rational design of pressure sensors for specific target applications (Figure 16). In general, the rapid growth of this field promises to not only meet the growing need for specialization but also to expand pressure sensors into new and exciting application areas.

## Acknowledgements

This project is supported by the Beijing Institute of Collaborative Innovation. V.R.F. was supported by the Department of Defense (DoD) through the National Defense Science & Engineering Graduate (NDSEG) Fellowship Program. H.T. was supported by an appointment to the Intelligence Community Postdoctoral Research Fellowship Program at Stanford University, administered by Oak Ridge Institute for Science and Education through an interagency agreement between the U.S. Department of Energy and the Office of the Director of National Intelligence.

## Conflict of Interest

The authors declare no conflict of interest.

## Keywords

active layers, microengineering, pressure sensors, sensor performance

Received: April 21, 2020

Revised: May 18, 2020

Published online:

- [1] Y. Hao, R. Foster, *Physiol. Meas.* **2008**, *29*, R27.
- [2] A. Pantelopoulou, N. G. Bourbakis, *IEEE Trans. Syst. Man Cybern., Part C (Appl. Rev.)* **2010**, *40*, 1.
- [3] A. Billard, D. Kragic, *Science* **2019**, *364*, eaat8414.
- [4] J. C. Yang, J. Mun, S. Y. Kwon, S. Park, Z. Bao, S. Park, *Adv. Mater.* **2019**, *31*, 1904765.
- [5] Z. Liu, Y. Ma, H. Ouyang, B. Shi, N. Li, D. Jiang, F. Xie, D. Qu, Y. Zou, Y. Huang, H. Li, C. Zhao, P. Tan, M. Yu, Y. Fan, H. Zhang, Z. L. Wang, Z. Li, *Adv. Funct. Mater.* **2018**, *29*, 1807560.
- [6] C. M. Boutry, A. Nguyen, Q. O. Lawal, A. Chortos, S. Rondeau-Gagné, Z. Bao, *Adv. Mater.* **2015**, *27*, 6954.
- [7] K. Meng, J. Chen, X. Li, Y. Wu, W. Fan, Z. Zhou, Q. He, X. Wang, X. Fan, Y. Zhang, J. Yang, Z. L. Wang, *Adv. Funct. Mater.* **2018**, *29*, 1806388.
- [8] G. Schwartz, B. C.-K. Tee, J. Mei, A. L. Appleton, D. H. Kim, H. Wang, Z. Bao, *Nat. Commun.* **2013**, *4*, 1859.
- [9] W. T. Abraham, P. B. Adamson, R. C. Bourge, M. F. Aaron, M. R. Costanzo, L. W. Stevenson, W. Strickland, S. Neelagaru, N. Raval, S. Krueger, S. Weiner, D. Shavelle, B. Jeffries, J. S. Yadav, *Lancet* **2011**, *377*, 658.
- [10] C. M. Boutry, L. Beker, Y. Kaizawa, C. Vassos, H. Tran, A. C. Hinckley, R. Pfattner, S. Niu, J. Li, J. Claverie, Z. Wang, J. Chang, P. M. Fox, Z. Bao, *Nat. Biomed. Eng.* **2019**, *3*, 47.
- [11] C. M. Boutry, Y. Kaizawa, B. C. Schroeder, A. Chortos, A. Legrand, Z. Wang, J. Chang, P. Fox, Z. Bao, *Nat. Electron.* **2018**, *1*, 314.
- [12] S. Jung, J. Lee, T. Hyeon, M. Lee, D. H. Kim, *Adv. Mater.* **2014**, *26*, 6329.
- [13] P. Chen, D. C. Rodger, S. Saati, M. S. Humayun, Y. Tai, *J. Microelectromech. Syst.* **2008**, *17*, 1342.
- [14] T. Sharma, S. S. Je, B. Gill, J. X. J. Zhang, *Sens. Actuators, A* **2012**, *177*, 87.
- [15] S. C. B. Mannsfeld, B. C. K. Tee, R. M. Stoltenberg, C. V. H. H. Chen, S. Barman, B. V. O. Muir, A. N. Sokolov, C. Reese, Z. Bao, *Nat. Mater.* **2010**, *9*, 859.
- [16] G. Y. Bae, J. T. Han, G. Lee, S. Lee, S. W. Kim, S. Park, J. Kwon, S. Jung, K. Cho, *Adv. Mater.* **2018**, *30*, 1803388.
- [17] B. C. K. Tee, A. Chortos, R. R. Dunn, G. Schwartz, E. Eason, Z. Bao, *Adv. Funct. Mater.* **2014**, *24*, 5427.
- [18] I. You, S. E. Choi, H. Hwang, S. W. Han, J. W. Kim, U. Jeong, *Adv. Funct. Mater.* **2018**, *28*, 1801858.
- [19] Q. Sun, D. H. Kim, S. S. Park, N. Y. Lee, Y. Zhang, J. H. Lee, K. Cho, J. H. Cho, *Adv. Mater.* **2014**, *26*, 4735.
- [20] D. Kwon, T. I. Lee, J. Shim, S. Ryu, M. S. Kim, S. Kim, T. S. Kim, I. Park, *ACS Appl. Mater. Interfaces* **2016**, *8*, 16922.
- [21] M. Ramuz, B. C. K. Tee, J. B. H. Tok, Z. Bao, *Adv. Mater.* **2012**, *24*, 3223.
- [22] C. Wang, D. Hwang, Z. Yu, K. Takei, J. Park, T. Chen, B. Ma, A. Javey, *Nat. Mater.* **2013**, *12*, 899.
- [23] G. Yu, J. Hu, J. Tan, Y. Gao, Y. Lu, F. Xuan, *Nanotechnology* **2018**, *29*, 115502.



- [24] C. Yang, L. Li, J. Zhao, J. Wang, J. Xie, Y. Cao, M. Xue, C. Lu, *ACS Appl. Mater. Interfaces* **2018**, 10, 25811.
- [25] Z. Yu, G. Cai, P. Tong, D. Tang, *ACS Sens.* **2019**, 4, 2272.
- [26] J. M. Smit, C. J. Zeebregts, R. Acosta, P. M. N. Werker, *Plast. Reconstr. Surg.* **2010**, 125, 177.
- [27] S. J. Lin, M. D. Nguyen, C. Chen, S. Colakoglu, M. S. Curtis, A. M. Tobias, B. T. Lee, *Plast. Reconstr. Surg.* **2011**, 127, 1080.
- [28] R. S. Dahiya, M. Valle, *Sensors: Focus Tactile Force Stress Sensors*, InTech, London **2008**.
- [29] Y. Gao, H. Ota, E. W. Schaler, K. Chen, A. Zhao, W. Gao, H. M. Fahad, Y. Leng, A. Zheng, F. Xiong, C. Zhang, L. C. Tai, P. Zhao, R. S. Fearing, A. Javey, *Adv. Mater.* **2017**, 29, 1701985.
- [30] W. Hu, X. Niu, R. Zhao, Q. Pei, *Appl. Phys. Lett.* **2013**, 102, 083303.
- [31] D. J. Lipomi, M. Vosgueritchian, B. C.-K. Tee, S. L. Hellstrom, J. A. Lee, C. H. Fox, Z. Bao, *Nat. Nanotechnol.* **2011**, 6, 788.
- [32] J. Zhang, L. J. Zhou, H. M. Zhang, Z. X. Zhao, S. L. Dong, S. Wei, J. Zhao, Z. L. Wang, B. Guo, P. A. Hu, *Nanoscale* **2018**, 10, 7387.
- [33] T. Yang, D. Xie, Z. Li, H. Zhu, *Mater. Sci. Eng., R* **2017**, 115, 1.
- [34] H. B. Muhammad, C. Recchiuto, C. M. Oddo, L. Beccai, C. J. Anthony, M. J. Adams, M. C. Carrozza, M. C. L. Ward, *Microelectron. Eng.* **2011**, 88, 1811.
- [35] C. Yeom, K. Chen, D. Kiriya, Z. Yu, G. Cho, A. Javey, *Adv. Mater.* **2015**, 27, 1561.
- [36] C. Li, P. M. Wu, S. Lee, A. Gorton, M. J. Schulz, C. H. Ahn, *J. Microelectromech. Syst.* **2008**, 17, 334.
- [37] S. Bauer, S. Bauer-Gogonea, I. Graz, M. Kaltenbrunner, C. Keplinger, R. Schwödiauer, *Adv. Mater.* **2014**, 26, 149.
- [38] W. Choi, J. Lee, Y. Kyoung Yoo, S. Kang, J. Kim, J. Hoon Lee, *Appl. Phys. Lett.* **2014**, 104, 123701.
- [39] X. Wang, L. Dong, H. Zhang, R. Yu, C. Pan, Z. L. Wang, *Adv. Sci.* **2015**, 2, 1500169.
- [40] R. S. Dahiya, G. Metta, M. Valle, G. Sandini, *IEEE Trans. Rob.* **2010**, 26, 1.
- [41] M. E. H. Eltaib, J. R. Hewit, *Mechatronics* **2003**, 13, 1163.
- [42] S. Lim, D. Son, J. Kim, Y. B. Lee, J. K. Song, S. Choi, D. J. Lee, J. H. Kim, M. Lee, T. Hyeon, D. H. Kim, *Adv. Funct. Mater.* **2015**, 25, 375.
- [43] G. Zhu, W. Q. Yang, T. Zhang, Q. Jing, J. Chen, Y. S. Zhou, P. Bai, Z. L. Wang, *Nano Lett.* **2014**, 14, 3208.
- [44] S. Jung, J. H. Kim, J. Kim, S. Choi, J. Lee, I. Park, T. Hyeon, D. H. Kim, *Adv. Mater.* **2014**, 26, 4825.
- [45] Y. Xiong, Y. Shen, L. Tian, Y. Hu, P. Zhu, R. Sun, C. P. Wong, *Nano Energy* **2020**, 70, 104436.
- [46] B. C.-K. Tee, A. Chortos, A. Berndt, A. K. Nguyen, A. Torn, A. McGuire, Z. C. Lin, K. Tien, W.-G. Bae, H. Wang, P. Mei, H.-H. Chou, B. Cui, K. Deisseroth, T. Nga Ng, Z. Bao, *Science* **2015**, 350, 313.
- [47] IEEE, *IEEE Standard for Sensor Performance Parameter Definitions*, IEEE Electron Devices Society, New York **2017**.
- [48] Z. Liu, L. Htein, K.-K. Lee, K.-T. Lau, H.-Y. Tam, *Sci. Rep.* **2018**, 8, 65.
- [49] M. L. Hammock, A. Chortos, B. C. K. Tee, J. B. H. Tok, Z. Bao, *Adv. Mater.* **2013**, 25, 5997.
- [50] M. Stoppa, A. Chiolerio, *Sensors* **2014**, 14, 11957.
- [51] L. M. Castano, A. B. Flatau, *Smart Mater. Struct.* **2014**, 23, 053001.
- [52] T. H. N. Dinh, P.-Y. Joubert, E. Martincic, E. Dufour-Gergam, in *2014 IEEE Int. Symp. on Medical Measurements and Applications (MeMeA)*, IEEE, Lisboa **2014**, p. 1.
- [53] J. Kim, T. Nga Ng, W. Soo Kim, *Appl. Phys. Lett.* **2012**, 101, 103308.
- [54] A. M. Almassri, W. Z. Wan Hasan, S. A. Ahmad, A. J. Ishak, A. M. Ghazali, D. N. Talib, C. Wada, *J. Sens.* **2015**, 2015, 846487.
- [55] A. Nallathambi, T. Shanmuganathan, D. Sindhanaiselvi, *Mater. Today: Proc.* **2018**, 5, 1897.
- [56] S. Jung, J. H. Kim, J. Kim, S. Choi, J. Lee, I. Park, T. Hyeon, D. H. Kim, *Adv. Mater.* **2014**, 26, 4825.
- [57] A. V. Shirinov, W. K. Schomburg, *Sens. Actuators, A* **2008**, 142, 48.
- [58] X. Wang, T. Li, J. Adams, J. Yang, *J. Mater. Chem. A* **2013**, 1, 3580.
- [59] F. Xu, Y. Zhu, *Adv. Mater.* **2012**, 24, 5117.
- [60] D. P. J. Cotton, I. M. Graz, S. P. Lacour, *IEEE Sens. J.* **2009**, 9, 2008.
- [61] L. Lin, Y. Xie, S. Wang, W. Wu, S. Niu, X. Wen, Z. L. Wang, *ACS Nano* **2013**, 7, 8266.
- [62] P. S. Das, A. Chhetry, P. Maharjan, M. S. Rasel, J. Y. Park, *Nano Res.* **2019**, 12, 1789.
- [63] T. Zhao, T. Li, L. Chen, L. Yuan, X. Li, J. Zhang, *ACS Appl. Mater. Interfaces* **2019**, 11, 29466.
- [64] N. Bai, L. Wang, Q. Wang, J. Deng, Y. Wang, P. Lu, J. Huang, G. Li, Y. Zhang, J. Yang, K. Xie, X. Zhao, C. F. Guo, *Nat. Commun.* **2020**, 11, 209.
- [65] J. He, Y. Zhang, R. Zhou, L. Meng, T. Chen, W. Mai, C. Pan, *J. Mater.* **2020**, 6, 86.
- [66] R. Puers, *Sens. Actuators, A* **1993**, 37-38, 93.
- [67] S. Kang, J. Lee, S. Lee, S. G. Kim, J. K. Kim, H. Algadi, S. Al-Sayari, D. E. Kim, D. E. Kim, T. Lee, *Adv. Electron. Mater.* **2016**, 2, 1600356.
- [68] M. Y. Cheng, C. L. Lin, Y. T. Lai, Y. J. Yang, *Sensors* **2010**, 10, 10211.
- [69] R. D. Ponce Wong, J. D. Posner, V. J. Santos, *Sens. Actuators, A* **2012**, 179, 62.
- [70] J. A. Dobrzynska, M. A. M. Gijs, *Sens. Actuators, A* **2012**, 173, 127.
- [71] S. R. A. Ruth, L. Beker, H. Tran, V. R. Feig, N. Matsuhisa, Z. Bao, *Adv. Funct. Mater.* **2019**, 1903100.
- [72] K. A. Mathias, S. M. Kulkarni, *IOP Conf. Ser.: Mater. Sci. Eng.* **2018**, 417, 012035.
- [73] Q. Su, X. Huang, K. Lan, T. Xue, W. Gao, Q. Zou, *J. Micromech. Microeng.* **2020**, 30, 015009.
- [74] S. Wang, K. H. Huang, Y. J. Yang, in *2019 20th Int. Conf. Solid-State Sensors, Actuators Microsystems Eurosensors XXXIII, TRANSDUCERS 2019 and EUROSENSORS XXXIII*, IEEE, Berlin **2019**, pp. 458–461.
- [75] J. C. Yang, J.-O. Kim, J. Oh, S. Y. Kwon, J. Y. Sim, D. W. Kim, H. B. Choi, S. Park, *ACS Appl. Mater. Interfaces* **2019**, 11, 19472.
- [76] J. Yang, S. Luo, X. Zhou, J. Li, J. Fu, W. Yang, D. Wei, *ACS Appl. Mater. Interfaces* **2019**, 11, 14997.
- [77] W. Deng, X. Huang, W. Chu, Y. Chen, L. Mao, Q. Tang, W. Yang, *J. Sens.* **2016**, 2016, 2428305.
- [78] H. H. Chou, A. Nguyen, A. Chortos, J. W. F. To, C. Lu, J. Mei, T. Kurosawa, W. G. Bae, J. B. H. Tok, Z. Bao, *Nat. Commun.* **2015**, 6, 8011.
- [79] Y. Joo, J. Byun, N. Seong, J. Ha, H. Kim, S. Kim, T. Kim, H. Im, D. Kim, Y. Hong, *Nanoscale* **2015**, 7, 6208.
- [80] X. Shuai, P. Zhu, W. Zeng, Y. Hu, X. Liang, Y. Zhang, R. Sun, C. P. Wong, *ACS Appl. Mater. Interfaces* **2017**, 9, 26314.
- [81] Y. Joo, J. Yoon, J. Ha, T. Kim, S. Lee, B. Lee, C. Pang, Y. Hong, *Adv. Electron. Mater.* **2017**, 3, 1600455.
- [82] Y. C. Huang, Y. Liu, C. Ma, H. C. Cheng, Q. He, H. Wu, C. Wang, C. Y. Lin, Y. Huang, X. Duan, *Nat. Electron.* **2020**, 3, 59.
- [83] L. Ma, X. Yu, Y. Yang, Y. Hu, X. Zhang, H. Li, X. Ouyang, P. Zhu, R. Sun, C. ping Wong, *J. Mater.* **2020**, 6, 321.
- [84] F. Liu, F. Han, L. Ling, J. Li, S. Zhao, T. Zhao, X. Liang, D. Zhu, G. Zhang, R. Sun, D. Ho, C. P. Wong, *Chem. - Eur. J.* **2018**, 24, 16823.
- [85] Y. Wan, Z. Qiu, Y. Hong, Y. Wang, J. Zhang, Q. Liu, Z. Wu, C. F. Guo, *Adv. Electron. Mater.* **2018**, 4, 1700586.
- [86] A. Chhetry, J. Kim, H. Yoon, J. Y. Park, *ACS Appl. Mater. Interfaces* **2019**, 11, 3438.
- [87] J. O. Kim, S. Y. Kwon, Y. Kim, H. B. Choi, J. C. Yang, J. Oh, H. S. Lee, J. Y. Sim, S. Ryu, S. Park, *ACS Appl. Mater. Interfaces* **2019**, 11, 1503.
- [88] C. Metzger, E. Fleisch, J. Meyer, M. Dansachmüller, I. Graz, M. Kaltenbrunner, C. Keplinger, R. Schwödiauer, S. Bauer, *Appl. Phys. Lett.* **2008**, 92, 013506.
- [89] P. Wei, X. Guo, X. Qiu, D. Yu, *Nanotechnology* **2019**, 30, 455501.

- [90] Y. Zhang, Z. Lin, X. Huang, X. You, J. Ye, H. Wu, *Smart Mater. Struct.* **2019**, *28*, 105023.
- [91] L. Feng, S. Li, Y. Li, H. Li, L. Zhang, J. Zhai, Y. Song, B. Liu, L. Jiang, D. Zhu, *Adv. Mater.* **2002**, *14*, 1857.
- [92] Y. Xia, G. M. Whitesides, *Annu. Rev. Mater. Sci.* **1998**, *28*, 153.
- [93] J. Wang, R. Suzuki, M. Shao, F. Gillot, S. Shiratori, *ACS Appl. Mater. Interfaces* **2019**, *11*, 11928.
- [94] M. I. Butrón-García, J. A. Jofre-Reche, J. M. Martín-Martínez, *Appl. Surf. Sci.* **2015**, *332*, 1.
- [95] C. Yu, H. Jiang, *Thin Solid Films* **2010**, *519*, 818.
- [96] S. M. Miriyala, Y. S. Kim, L. Liu, J. C. Grunlan, *Macromol. Chem. Phys.* **2008**, *209*, 2399.
- [97] S. Peng, P. Blanloeuil, S. Wu, C. H. Wang, *Adv. Mater. Interfaces* **2018**, *5*, 1800403.
- [98] Y. Pang, H. Tian, L. Tao, Y. Li, X. Wang, N. Deng, Y. Yang, T. L. Ren, *ACS Appl. Mater. Interfaces* **2016**, *8*, 26458.
- [99] C. L. Choong, M. B. Shim, B. S. Lee, S. Jeon, D. S. Ko, T. H. Kang, J. Bae, S. H. Lee, K. E. Byun, J. Im, Y. J. Jeong, C. E. Park, J. J. Park, U. I. Chung, *Adv. Mater.* **2014**, *26*, 3451.
- [100] M. Amjadi, K. U. Kyung, I. Park, M. Sitti, *Adv. Funct. Mater.* **2016**, *26*, 1678.
- [101] J. Park, Y. Lee, J. Hong, M. Ha, Y. Do Jung, H. Lim, S. Y. Kim, H. Ko, *ACS Nano* **2014**, *8*, 4689.
- [102] J. Park, Y. Lee, J. Hong, Y. Lee, M. Ha, Y. Jung, H. Lim, S. Y. Kim, H. Ko, *ACS Nano* **2014**, *8*, 12020.
- [103] Y. Pang, K. Zhang, Z. Yang, S. Jiang, Z. Ju, Y. Li, X. Wang, D. Wang, M. Jian, Y. Zhang, R. Liang, H. Tian, Y. Yang, T. L. Ren, *ACS Nano* **2018**, *12*, 2346.
- [104] L. Pan, A. Chortos, G. Yu, Y. Wang, S. Isaacson, R. Allen, Y. Shi, R. Dauskardt, Z. Bao, *Nat. Commun.* **2014**, *5*, 3002.
- [105] R. Guo, Y. Yu, J. Zeng, X. Liu, X. Zhou, L. Niu, T. Gao, K. Li, Y. Yang, F. Zhou, Z. Zheng, *Adv. Sci.* **2015**, *2*, 1400021.
- [106] M. Xu, Y. Gao, G. Yu, C. Lu, J. Tan, F. Xuan, *Sens. Actuators, A* **2018**, *284*, 260.
- [107] Y. Gao, C. Lu, G. Yu, J. Sha, J. Tan, F.-Z. Xuan, *Nanotechnology* **2019**, *30*, 325502.
- [108] H. Li, K. Wu, Z. Xu, Z. Wang, Y. Meng, L. Li, *ACS Appl. Mater. Interfaces* **2018**, *10*, 20826.
- [109] J. Shi, L. Wang, Z. Dai, L. Zhao, M. Du, H. Li, Y. Fang, *Small* **2018**, *14*, 1800819.
- [110] Y. Wei, S. Chen, Y. Lin, Z. Yang, L. Liu, *J. Mater. Chem. C* **2015**, *3*, 9594.
- [111] G. Y. Bae, S. W. Pak, D. Kim, G. Lee, D. H. Kim, Y. Chung, K. Cho, *Adv. Mater.* **2016**, *28*, 5300.
- [112] C. W. Visser, D. N. Amato, J. Mueller, J. A. Lewis, *Adv. Mater.* **2019**, *31*, 1904668.
- [113] Q. Tian, W. Yan, Y. Li, D. Ho, *ACS Appl. Mater. Interfaces* **2020**, *12*, 9710.
- [114] X. Chen, H. Liu, Y. Zheng, Y. Zhai, X. Liu, C. Liu, L. Mi, Z. Guo, C. Shen, *ACS Appl. Mater. Interfaces* **2019**, *11*, 42594.
- [115] Z. Wang, L. Zhang, J. Liu, H. Jiang, C. Li, *Nanoscale* **2018**, *10*, 10691.
- [116] Z. W. Shan, G. Adesso, A. Cabot, M. P. Sherburne, S. A. Syed Asif, O. L. Warren, D. C. Chrzan, A. M. Minor, A. P. Alivisatos, *Nat. Mater.* **2008**, *7*, 947.
- [117] G. Ge, Y. Cai, Q. Dong, Y. Zhang, J. Shao, W. Huang, X. Dong, *Nanoscale* **2018**, *10*, 10033.
- [118] A. Tewari, S. Gandla, S. Bohm, C. R. McNeill, D. Gupta, *ACS Appl. Mater. Interfaces* **2018**, *10*, 5185.
- [119] J. Jia, G. Huang, J. Deng, K. Pan, *Nanoscale* **2019**, *11*, 4258.
- [120] Y. Yu, C. Yan, Z. Zheng, *Adv. Mater.* **2014**, *26*, 5508.
- [121] W. Zhong, C. Liu, Q. Liu, L. Piao, H. Jiang, W. Wang, K. Liu, M. Li, G. Sun, D. Wang, *ACS Appl. Mater. Interfaces* **2018**, *10*, 42706.
- [122] X. Wu, Y. Han, X. Zhang, Z. Zhou, C. Lu, *Adv. Funct. Mater.* **2016**, *26*, 6246.
- [123] Y. Wang, M. Chao, P. Wan, L. Zhang, *Nano Energy* **2020**, *70*, 104560.
- [124] J. Oh, J. O. Kim, Y. Kim, H. B. Choi, J. C. Yang, S. Lee, M. Pyatykh, J. Kim, J. Y. Sim, S. Park, *Small* **2019**, *15*, 1901744.
- [125] H. B. Yao, G. Huang, C. H. Cui, X. H. Wang, S. H. Yu, *Adv. Mater.* **2011**, *23*, 3643.
- [126] C. Yang, Y. Xu, P. Man, H. Zhang, Y. Huo, C. Yang, Z. Li, S. Jiang, B. Man, *RSC Adv.* **2017**, *7*, 35016.
- [127] A. Kovalenko, K. Zimny, B. Mascaro, T. Brunet, O. Mondain-Monval, *Soft Matter* **2016**, *12*, 5154.
- [128] L. Yang, R. Wang, Q. Song, Y. Liu, Q. Zhao, Y. Shen, *Composites, Part A* **2017**, *101*, 195.
- [129] L. González, M. Baoguang, L. Li, J. H. Hansen, S. Hvilsted, A. L. Skov, *Macromol. Mater. Eng.* **2014**, *299*, 729.
- [130] S. Miller, Z. Bao, *J. Mater. Res.* **2015**, *30*, 3584.
- [131] M. Wegener, W. Wirges, R. Gerhard-Multhaupt, *Adv. Eng. Mater.* **2005**, *7*, 1128.
- [132] M. G. Broadhurst, G. T. Davis, *Ferroelectrics* **1984**, *60*, 3.
- [133] C. Pan, Z. Li, W. Guo, J. Zhu, Z. L. Wang, *Angew. Chem., Int. Ed.* **2011**, *50*, 11192.
- [134] J. H. Lee, H. J. Yoon, T. Y. Kim, M. K. Gupta, J. H. Lee, W. Seung, H. Ryu, S. W. Kim, *Adv. Funct. Mater.* **2015**, *25*, 3203.
- [135] V. V. Kochervinski, *Crystallogr. Rep.* **2003**, *48*, 649.
- [136] W. Zeng, X. M. Tao, S. Chen, S. Shang, H. L. W. Chan, S. H. Choy, *Energy Environ. Sci.* **2013**, *6*, 2631.
- [137] J. Chun, K. Y. Lee, C. Y. Kang, M. W. Kim, S. W. Kim, J. M. Baik, *Adv. Funct. Mater.* **2014**, *24*, 2038.
- [138] S. Chen, N. Wu, L. Ma, S. Lin, F. Yuan, Z. Xu, W. Li, B. Wang, J. Zhou, *ACS Appl. Mater. Interfaces* **2018**, *10*, 3660.
- [139] X. Chen, X. Li, J. Shao, N. An, H. Tian, C. Wang, T. Han, L. Wang, B. Lu, *Small* **2017**, *13*, 1604245.
- [140] L. Lin, S. Wang, Y. Xie, Q. Jing, S. Niu, Y. Hu, Z. L. Wang, *Nano Lett.* **2013**, *13*, 2916.
- [141] S. Wang, L. Lin, Z. L. Wang, *Nano Lett.* **2012**, *12*, 6339.
- [142] F. R. Fan, Z. Q. Tian, Z. L. Wang, *Nano Energy* **2012**, *1*, 328.
- [143] B. A. Grzybowski, A. Winkleman, J. A. Wiles, Y. Brumer, G. M. Whitesides, *Nat. Mater.* **2003**, *2*, 241.
- [144] A. F. Diaz, R. M. Felix-Navarro, *J. Electroanal. Chem.* **2004**, *562*, 277.
- [145] G. Zhu, C. Pan, W. Guo, C. Y. Chen, Y. Zhou, R. Yu, Z. L. Wang, *Nano Lett.* **2012**, *12*, 4960.
- [146] S. Niu, Z. L. Wang, *Nano Energy* **2015**, *14*, 161.
- [147] F. Yi, L. Lin, S. Niu, P. K. Yang, Z. Wang, J. Chen, Y. Zhou, Y. Zi, J. Wang, Q. Liao, Y. Zhang, Z. L. Wang, *Adv. Funct. Mater.* **2015**, *25*, 3688.
- [148] A. Chortos, J. Liu, Z. Bao, *Nat. Mater.* **2016**, *15*, 937.